MUHAMMAD HARIS LATIF

por Humair Abbas

Fecha de entrega: 28-ene-2021 05:41a.m. (UTC+0100)
Identificador de la entrega: 1496030076
Nombre del archivo: Thesis.docx (7.01M)
Total de palabras: 15074
Total de caracteres: 86444

T.C.

ANTALYA BILIM UNIVERSITY INSTITUTE OF POSTGRADUATE EDUCATION OF ELECTRICAL AND COMPUTER ENGINEERING

THESIS PROGAM

THEORETICAL ANALYSIS AND SIMULATIONS ON THE DEVELOPMENT OF AN ULTRASONIC BIOSENSOR FOR THE DETECTION OF ARTERIAL RUPTURE

DISSERTATION

Prepared By

Muhammad Haris LATIF

ANTALYA – 2021

T.C.
ANTALYA BILIM UNIVERSITY INSTITUTE OF
POSTGRADUATE EDUCATION OF ELECTRICAL AND
COMPUTER ENGINEERING

THESIS PROGAM

THEORETICAL ANALYSIS AND SIMULATIONS ON THE DEVELOPMENT OF AN ULTRASONIC BIOSENSOR FOR THE DETECTION OF ARTERIAL RUPTURE

DISSERTATION

Prepared By

Muhammad Haris LATIF

Dissertation Advisor

Asst. Prof. Dr. Mustafa İlker BEYAZ

ANTALYA – 2021

INSTITUTE OF POSTGRADUATE EDUCATION

ELECTRICAL AND COMPUTER ENGINEERING

MASTER PROGRAM WITH THESIS

ACADEMIC DECLATION

I hereby declare that this master's thesis titled "Theoretical analysis and simulations on the development of an ultrasonic biosensor for the detection of arterial rupture" has been written by myself under the academic rules and ethical conduct of the Antalya Bilim University.

I also declare that the work attached to this declaration complies with the university requirements and is my work.

I also declare that all materials used in this thesis consist of the mentioned resources in the reference list. I verify all these with my honor.

… / … / 2021

Muhammad Haris Latif

APPROVAL/NOTIFICATION FORM

ANTALYA BİLİM UNIVERSİTY

INSTITUTE OF POST-GRADUATE EDUCATION

MUHAMMAD HARIS LATIF, is a M.Sc. student of Antalya Bilim University, Institute of Post Graduate Education, Electrical and Computer Engineering owning student ID 181212016, successfully defended the thesis/dissertation entitled "Theoretical analysis and simulations on the development of an ultrasonic biosensor for the detection of arterial rupture" which he prepared after fulfilling the requirements specified in the associated legislations, before the jury whose signatures are below.

Academic Tittle, Name-Surname, Signature

Jury Member (Chairman) : ……,……..

Jury Member : ……,……..

Jury Member :……,……..

Date of Submission: 25/12/2020

Date of Defense: 11/01/2021

Director of the Institute : ……..

ÖZET

THEORETICAL ANALYSIS AND SIMULATIONS ON THE DEVELOPMENT OF AN ULTRASONIC BIOSENSOR FOR THE DETECTION OF ARTERIAL RUPTURE

Anevrizma, uzun süreli yüksek tansiyon ve arter duvarındaki yüksek elastikiyetin neden olduğu, arterin şişmesi ile ilgili bir hastalıktır. Genellikle bu hastalıkla ilişkili hiçbir belirti yoktur. Bununla birlikte, uzun süreli bir anevrizma ölümcül ve tehlikeli olabilir ve bu da hayatı tehdit eden iç kanamaya yol açar. Bir hastada bir anevrizma tespit edildiğinde, bu hastalığa karşı koymak için en iyi yaklaşım, bir artere stent eklemektir. Stent yerleştirilmesi genç hastalar için oldukça basit olabilir ancak yaşlı insanlar için hayati riskler oluşturabilir. Bu nedenle, atardamar yırtılmaya başlayana kadar ameliyatı beklemek en iyisi olabilir. Bekleme süresi hastanın durumuna bağlıdır ve her hasta için aylardan birkaç yıla kadar değişebilir. Arter yırtılmaya başladığında hayati risk kaçınılmaz olduğundan stent işlemi uygulanmalıdır. Bu araştırma kapsamında, arterin yırtılmaya başladığı bu olası son anı tespit edebilen bir sensör tasarımı geliştirdi. Bu sensör, koroner arter stentinin yerleştirilmesiyle ilgili riskleri geciktirerek cerrahi prosedürü önlemek için hastalara mümkün olan maksimum süreyi tanır. Bu sensör tam olarak uygulandığında, arter yırtılması erken tespit edilebilir ve mortalite önlenebilir, hastaya daha uzun, ameliyatsız ve konforlu bir yaşam sağlanır. Bu cihazın anevrizma yeri ile aynı hizada cilt üzerine yerleştirilmesi öngörülmüştür. Sensör tarafından alınan ve işlenen sinyaller, her yırtılma boyutu için farklı olacak, bu da doktorun yukarıda belirtilen durumlara göre ilerleyebilmesi için yırtılma boyutu hakkında fikir verecektir. Sensör tasarımı COMSOL üzerinde uygulanmış ve arter yırtılmasını tespit etmek için farklı frekans değerleri için simüle edilmiştir. Normal ve yırtılmış arterin ultrasonik ekolarının frekans spektrumları arasında önemli bir fark gözlemlenmiştir. Sonuçlara dayanarak, bir piezoelektrik dönüştürücü geometrisi, 10 MHz frekansında ultrasonik sinyaller göndermek ve almak için tasarlanmıştır. Cihazın üretimi için gerekli üretim prosedürleri belirlenmiştir.

Anahtar kelime: Biyosensörler, ultrasonik, Anevrizma, Arter, Yırtılma,

ABSTRACT

THEORETICAL ANALYSIS AND SIMULATIONS ON THE DEVELOPMENT OF AN ULTRASONIC BIOSENSOR FOR THE DETECTION OF ARTERIAL RUPTURE

An aneurysm is a disease related to an artery's distention, which is caused by prolonged high blood pressures and the high elasticity in the artery wall. There are usually no symptoms associated with this disease. However, a long-term aneurysm can be fatal and dangerous, which leads to life-threatening internal bleeding. When an aneurysm is detected in a patient, the best approach to counter this disease is by adding a stent to an artery. The stent insertion may be rather straight-forward for young patients but may pose vital risks for older people. Therefore, it may be best to wait for the surgery until the artery starts rupturing. The waiting period depends on the patient's condition and may vary for each patient from months to several years. When the artery starts rupturing, the stent procedure should be applied since the vital risk is unavoidable. This research has developed a sensor design that can detect this last possible moment when the artery starts rupturing. This sensor will delay the risks related to a coronary artery stent's insertion, giving the maximum possible time to prevent the surgical procedure. When this sensor is fully implemented, the artery rupture can be detected early, and mortality can be prevented, providing a longer, surgery-free, and comfortable life to a patient. This device is envisioned to be placed on the skin aligned with the aneurysm location. The signals received and processed by this sensor will be different for each rupture size, which will provide an idea about rupture size so that the doctor can proceed according to the situations mentioned above. The sensor design was developed on the COMSOL and simulated for different frequency values to detect the artery rupture. A significant difference between the frequency spectrums of the normal and ruptured artery's ultrasonic echoes was observed. Based on the results, a piezoelectric transducer geometry was designed to send and receive ultrasonic signals at an MHz range frequency. Necessary fabrication procedures to manufacture the device were determined.

Keyword: Biosensors, ultrasonics, Aneurysm, Arterial, Rupture.

DEDICATION AND ACKNOWLEDGMENT

I dedicate this thesis to my parents, friends, and teachers who always supported me to this day of my life.

I am very grateful to my advisor Assist. Prof. Dr. Mustafa İlker BEYAZ guided and encouraged me throughout the thesis. I would also like to thank the jury members Asst. Prof. Dr. Yusuf Öztürk and Asst. Prof. Dr. Deniz Kaya.

LIST OF TABLES

LIST OF FIGURES

ABBREVIATIONS

BOD	: Biochemical oxygen demand
DNA	: Deoxyribonucleic acid
CGM	: Continues glucose monitoring
CCD	: Charge-coupled device
MEMS	: Micro-electromechanical systems
CF	: Cystic fibrosis
ACG	: Acoustocerebrography
AAA	: Aorta abdomen's aneurysm
TAA	: Thoracic aorta aneurysm
SAH	: Subarachnoid hemorrhage
SPR	: Surface plasmon resonance
BAW	: Bulk acoustic wave
TSM	: Thickness shear mode
BL	: Bioluminescent
MRSA	: Methicillin-resistant staphylococcus aureus
DRN	: Direct radiation force
USW	: Ultrasonic standing wave
SAW	: Surface acoustic wave
HPSW	: Horizontally polarized shear waves
FBAR	: Film bulk acoustic resonators
HIFU	: High intensity focused beams
MRI	: Magnetic resonance imaging
FDA	: Food and drug administration
PDES	: Partial differential equation system
IDE	: Investigational device exemption

INDEX

INTRODUCTION

1. Definition

Ultrasonic energy can be produced and sensed by ultrasonic devices. They can be divided into three groups: transmitters, receivers, and transceivers. The working principle of ultrasonic devices is based on short wavelength and high-frequency sound waves, higher than 20,000 Hz frequencies, that are beyond the range that can be detected by the human ear.

1.1. Ultrasonic sensors

An ultrasonic sensor is an instrument that uses ultrasonic waves to determine the distance between the target and the source. It operates by transmitting an ultrasonic wave at a given frequency and obtaining the wave reflected from the target. Distance is calculated between the sensor and the object by using the formula is given below:

$$D = C_s \, {}^{t}/_{2} \qquad (1)$$

Here D is the distance between the emitter and recipient, t is travel time, and C_s in the air the sound speed is 343 m/s.

1.2. History

The biosensors are now omnipresent in biomedical diagnosis and a wide variety of other fields, including point-of-care management, disease development, environmental analysis, nutrient regulation, drug development, forensics, and biomedical science.

a wide range of biosensor's variety in applications to enhance life quality, such as detection in the disease, food safety, defiance, and discovery of the drug. One of the critical bio-sensor's applications is identifying biomolecules that are either disease markers or treatment targets. For example, electrochemical biosensing techniques can be used as clinical tools to detect protein cancer biomarkers.

1.2.1. Commercial Biosensors

The detection of changes in biological processes and converting them into electric signals is called biosensing. Accordingly, a device that can perform such functions is called a biosensor. Any organism or substance such as enzymes, tissues, microbes, cells, and acids can be considered a biological processor, where a biosensor can be used or integrated. Below is a simplified block diagram showing the typical building blocks of biosensors.

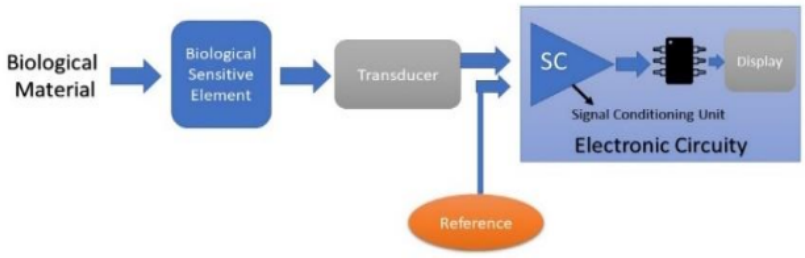

Figure 1: A biosensor device scheme

Figure. 1 shows the signal conditioning unit that contains an amplifier and a filter (usually a low case) circuitry. This block diagram illustrates a biosensor example, which will be described in detail in the following coming sections.

In advanced medicinal chemistry, chemicals and biosensors have more importance than other materials. There is a great diversity of approaches and techniques applied with the help of published research work. This wide variety is induced by new demands and opportunities, particularly in clinical diagnostics, environmental analysis, food analysis, and production surveillance [1][2]. The working theory of a sensor is to produce a signal that is proportional to the presence of specific biological events or intervening species of a particular (bio) chemical or a fixed (bio) chemical [3]. The use of sensitive instruments to accomplish this work using biological detection elements such as enzymes, tissues, and microorganisms is more effective because of its selective functionality.

Figure 2 illustrates biosensor's practical concepts. In terms of sensing area and transduction, sensors are separated into different categories depending on feature mode.

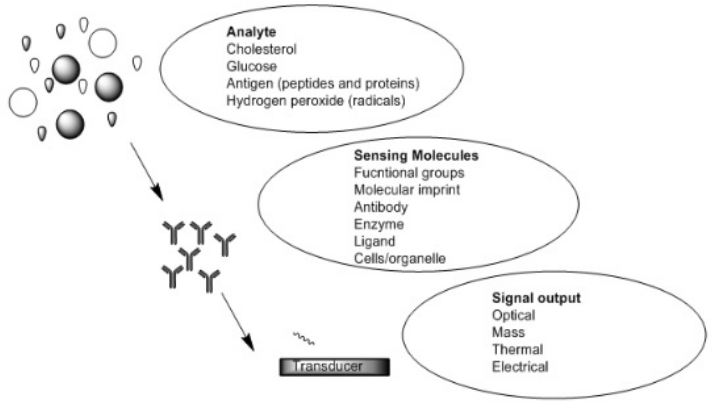

Figure 2: The functional principles of a biosensor.

1.2.2. Immunoassays biosensors

The immunoassays are bioanalytical techniques used to identify and measure the specificity of an antigen-antibody response in biological samples. These techniques are also used in clinical diagnosis, medication findings, drug discovery, and food testing. A theory of immunoassay is based on the competition between a constant amount of labeled analyte and a variable amount of unlabelled sample analysis to bind a small number of binding sites of an antibody directly raised against the analyte. These approaches are used to quantitatively, semi-quantitatively, or qualitatively detect a target molecule.

Figure 3: Immunoassay analyzer device [4]

Figure 3 shows the PATHFAST immunoassay analyzer device. PATHFAST is an easy-to-use, immunoassay bench-top analyzer that provides affordable, key lab-quality results from entire blood samples in less than 17 minutes.

1.2.3. Body Temperature sensor

A temperature sensor is an electronic device that monitors its environment temperature and transforms input data into electronic data for tracking, monitoring, or signal changes. Many different temperature sensors are available in the market. In specific locations in the body, the body temperature can be determined. The mouth, ear, armpit, and rectum are the most common body parts for detecting temperature. Body temperature is displayed in thermometers at either degree Fahrenheit (°F) or degree Celsius (°C).

Figure 4: Body temperature sensor [5]

Figure 4 illustrates a body temperature sensor, to determine the temperature of the human forehead. Recently, there've been significant improvements in human body temperature recording worldwide.

1.2.4. Biochemical oxygen demand (BOD) biosensor

Film biosensors are dependent on oxygen demand. Biochemical oxygen demand (BOD) sensors are microbial film sensors that rely on entire cells. The operation depends on the calculation of the oxygen intake by immobilized microorganisms on the transducer's surface. BOD measures the amount of oxygen in the decomposition of organic matter in the stream water consumed by microorganisms. BOD also tests inorganic material chemical oxidation (i.e., oxygen extraction from the water by chemical reactions).

Figure 5: BOD biosensor [6]

Figure 5 illustrates a BOD biosensor device developed by Proteus. The Proteus is a brand-new multiple-parameter BOD, COD, TOC, and Coliform (total, e.g., Coli or fecal) sensor platform that offers temperature and turbidity compensation in real-time.

1.2.5. Colorimetry biosensor

Colorimetry biosensors are used to assess colored compound concentration in solution. Sensitive and convenient picomolar levels of target DNA are freely identified with the naked eye, using this hybridization detection mechanism. The sensor works fine when faced with complex sample matrices like serum blood. Colorimetric gold nanoparticle biosensors have seen critical diagnostic applications.

Figure 6: Colorimetry device [7]

Figure 6 shows the tooth colorimetry device that can measure the color spectrum of teeth and crowns.

1.2.6. Glucose biosensor

The main concept of glucose biosensor is to immobilized GOx catalyzes, β-D glucose oxidation with molecular oxygen that produces gluconic acid and hydrogen peroxide. A glucose sensor is a continuous monitoring device for glucose (CGM) and implanted under the skin to measure glucose level. It transfers one's glucose data wirelessly to CGM system recipient or a compatible cognitive computer, allowing to control blood sugar levels at frequent intervals and make more educated medical decisions.

Figure 7: Glucose biosensor device [8]

Figure 7 shows the Glucose measuring device. That can be used for testing the concentration of glucose in the blood (glycemia).

1.2.7. Charge-coupled device (CCD) biosensor

A charge-coupled device (CCD) is an integrated circuit made on a silicon surface. Photons on this surface produce a charge that electronics can read and convert to a digital copy of the device's light patterns. CCDs are used in astronomy, microscopy, and biomedical imagery because of their high sensitivity overexposure periods. CCDs are related instruments of analog devices. Their charges are similar to the colors of light used in color filters for monochrome pictures or red, green, and blue colors.

Figure 8: CCD digital sensor. [9]

Figure 8 shows the CCD digital sensor used in digital intraoral x-ray provides a dental practice with a range of advantages in traditional film x-rays.

1.2.8. Pressure sensor

A pressure sensor is a gaseous or liquid pressure monitoring unit. Pressure refers to the force needed to avoid expanding a fluid, which is generally indicated in force per unit area. A pressure sensor usually serves as a transducer; it produces a signal centred on the applied intensity.

Figure 9: Blood pressure measuring device [10]

Figure 9 Shows a Blood Pressure measuring device. This device is used to measure blood pressure and heartbeat.

Blood pressure in different anatomical locations contains essential information. Pressure proximal and distal to the occlusion may be assessed to calculate the flow reserve magnitude. During a balloon catheter operation, blood pressure can also be evaluated. There are MEMS catheter pressure sensors which have benefits over fluid-filled catheters with external transducers. It doesn't have a catheter whip, minimal frequency response, and resonance. These sensors can penetrate small environment with pressures comparable to reference sensors because of their small scale. Continuous pressure control on cardiovascular products using wireless implantable microsystems provided potential capacity for heart failure, coronary artery disease, aneurysm, hypertension, and math for improved care and increased quality of life. This sensor is constructed of a flexible plate with an inductor winding attached to a hermetically sealed cavity (along with related dispersed capacities). Inductor windings fulfill two goals: (a) creating a resonant electrical circuit with a condenser and (b) magnetic connection with an external coil. A variation in the sensor strain affects the plates' location, increasing the sensor capacities and resonant frequency. The resonant frequency difference induces a shift in the external loop response regulated by external electronics.

1.3. Ultrasonic sensors

An ultrasonic sensor is a device that measures the distance of a target by releasing ultrasound waves and transforms reflected sound into an electrical signal. Humans cannot detect ultrasonic sounds because of their upper audible limit. Two critical components of the ultrasonic sensor are the transmitter (which transmits the sound using piezoelectric crystals) and the receiver. The sensor calculates the time it takes for the sound to travel between the transmitter and the receiver to determine the distance between the sensor and target. The approximation formula is given in eq (1). For instance, if one installs a box-orientated ultrasound sensor that takes 0.025 seconds for the sound to bounce back, the distance from the ultrasound sensor to the box will be:

$$D = 0.5 * 0.025 * 343 = 4.2875\text{m}$$

1.3.1.Medical ultrasound transducer

A medical ultrasound transducer is a portable device, used on over the patient's body. It is connected to a computer by the cord, and the device transmits sound waves and receives

the echoes as they bounce off the patient's body tissue and organs. The computer uses these echoes to create an image. Transducers are available in various sizes and shapes to use in different body areas. Some are positioned on or over the body, while others are created to fit into an opening.

Figure 10: Ultrasound transducer [11]

Figure 10 shows an ultrasound transducer device developed by Philips. That can use tissue aberration correction on transduces, body contrast-enhanced ultrasound for a more definitive diagnosis.

1.3.2. Ultrasound Image acquisition and display

Single ultrasound pulse-echo lines are called A-mode lines. The depth of the dispersed signal reflected or reversed is determined by knowledge of the tissue's sound speed and the time delay between signal transmission and received signals. The beam is swept through the area of interest by modifying each factor's exciting times in a range of transductors to generate a B-mode image. Although the array systems are electrically complex, the fast focus and multi-dimensional image acquisition are their main advantage. In B-mode visualization, stationary organs like kidney, breast, liver, or moving objects, such as a carotid artery, heart, or blood flow, are studied. Linear arrays are designed for high-resolution imaging of musculoskeletal or superficial vasculature. They are also used for calculating compound blood velocity (Sona CT) and Doppler. The 2-dimensional set can contain up to 2400 elements and create full-volume cardiological images. Arrays are beneficial because they

may focus on an entity or organ within the body by removing the components from receiving (phasing) signals. Three-dimensional volume imaging can be achieved by mechanically scanning a phased array transducer to each B-mode scan. Figure 10 reveals a traditional fetal two-dimensional image compared to a fetal three-dimensional volume picture.

Figure 11: Two-dimensional B-mode ultrasound image (left). Three-dimensional ultrasound image (right).

1.3.2.1. The Most Common Use of Ultrasound: Internal Imaging

In the field of medicine, the image produced by ultrasound is very important. Four different types of ultrasound imaging are available.

1. **A-mode**: In a single line, a single transducer scans the body. The echos are drawn as a function of depth.
2. **B-mode**: Produces a two-dimensional image in a linear array of transducers.

Figure 12: b-mode (two-dimensional image) [12].

3. **M-mode:** M-mode refers to motion in which a rapid series of B-mode scans gives details about targeted organ movement.

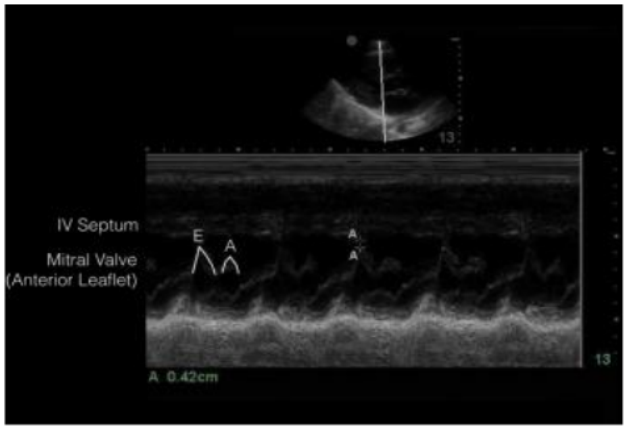

Figure 13: m-mode image [13].

4. **Doppler mode:** The doppler effect is used to measure blood flow and to visualize it.

   Typical applications include imaging various body regions, including the abdomen and the inner organs such as breasts/thyroid (neck), heart, vascular system, eyes, uterus.

   For example, ultrasound sensors are used to detect body organs such as the liver, kidneys, pancreas, and gallbladder, as well as to image internal organs located on the abdomen. Ultrasound sensors produce ultrasound frequencies between 2.5 MHz and 7.5 MHz using a linear array. Based on previous measurements, this gives a resolution of 0.2 mm to 0.6 mm. Moreover, in breast imaging, ultrasound sensors are often used to detect masses or assess a shapeshift. Physicians also use ultrasound to visualize the thyroid gland for mass checking. The sensors emit a higher frequency sound wave, usually between 7 MHz and 12 MHz.

   Further, cardiologists use ultrasound to assess the heart's size and shape and track valve movement inside the heart. Doppler effects may indicate blood flow direction, suggesting regurgitation and leakage aspects. Cardio-logical sensors run from 2 MHz to 7.5 MHz. Currently, blood flow sensors in the body typically rely on a higher frequency range, close to those used for the breast or thyroid test. Furthermore, in the internal imagery, the highest frequency waveform application occurs when examining the human eye, particularly before

cataract surgery. The determination of the length of the eye axis requires the greatest possible accuracy. For these ultrasound sensors, the core frequency range is between 10 and 22 MHz.

1.4. Motivation

Ultrasonic transduction has been used in many different prognostics, as described above. However, its application in the aneurysm is limited. Aneurysm disease occurs when part of an artery wall weakens, resulting in the artery's abnormal enlargement. To detect this condition of the artery, doctors apply different tests such as (ACG, CT scan, etc.). When an aneurysm is detected in a patient, the best approach to counter this disease is by adding a stent in the artery. The stent addition may be rather straight-forward for young patients but may pose vital risks for older people. Therefore, it may be best to wait for the surgery in some cases until the artery starts rupturing. The period of waiting depends on the patient's condition. It may vary for each patient from months to several years. When the artery starts rupturing, the stent procedure should be applied since the vital risk is unavoidable.

Our motivation is to develop a sensor that can detect this last possible moment when the artery starts rupturing. This sensor will delay the risks related to a coronary artery stent's insertion, giving the maximum possible time to prevent the surgical procedure. With this sensor's help, the artery rupture can be detected in the early stages, and mortality can be prevented, providing a longer surgery-free and comfortable life to a patient. In this research, an ultrasonic piezoelectric sensor that detects the artery rupture has been designed. The device is envisioned to be placed on the skin aligned with the aneurysm location. The signals received and processed by this sensor will be different for each rupture size, which will provide an idea about rupture size so that the doctor can proceed according to the situations mentioned above.

1.5. Novelty and Contribution

To the best of our knowledge, this is the first wearable on-skin ultrasonic sensor that detects the onset of rupture and the rupture size in the case of aneurysm disease. The device is designed to be portable and easy to use. This thesis focuses on the design and theoretical validation of the device through finite element simulations.

LITERATURE REVIEW

2. Ultrasound waves

The waves of ultrasound are generated by a transducer Ultrasound waves that can be emitted and ultrasound echoes detected. In some cases, the active components in ultrasound transducers are constructed of special piezoelectric ceramic crystal materials. As used in an electric field, such materials generate sound waves, and the reflected sound wave generates an electric field. When operating in an ultrasound scanner, a pulse of sound waves is transmitted through the body. The reflected sound waves represent tissue boundaries (e.g., The boundary between the liquid and the bone and soft tissue or tissue). When the transducer receives these echoes, they induce a voltage on the piezoelectric components. The scanner determines the distance from the transducer to the tissue boundary, using the speed of sound and the time of each echo return. In order to create tissue and organ representations in two dimensions, these distances are then used. During an ultrasound treatment, the technician adds a gel to the tissue. It stops air pockets between the transducer and the skin from forming and increases the coupling of ultrasound signals to the body.

2.1. **Diagnostic ultrasound**.

Diagnostic ultrasound, also known as sonography or medical diagnostic sonography, is used to produce body organ images using high-frequency sonic waves. These images provide valuable information for diagnosing and treating multiple disorders and diseases. Ultrasound diagnostic cannot invasively visualize the interior organs of the body. However, it is not suitable for imaging air-containing bones or tissues such as the lungs. In some conditions, the ultrasound can imagine bones or lungs and lining around the lungs when filled or partly filled with liquid (for example, in a small baby or a fetus). One of the most common use applications of ultrasound in fetal growth and pregnancy screening development. But other applications include cardiac imaging, blood vessels, eyes, thyroid, brain, breast, inner organs, skin, and muscles. Ultrasound images in 2D, 3D, or 4D are shown (4D in motion in figure 14).

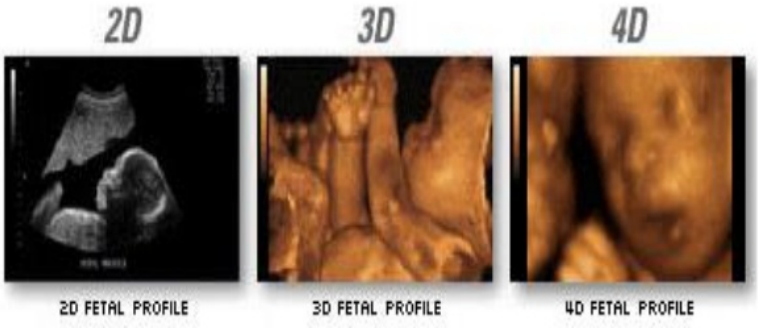

Figure 14:Ultrasound images [14].

2.2. Therapeutic ultrasound

Therapeutic ultrasounds produce a high acoustic output dependent on specific heat, ablating, or tissue breaking targets. One type of therapeutic ultrasound is a high intensity centred ultrasound with high-intensity focused beams (HIFU). HIFU is studied as a tool for modifying or destroying dysfunctional or diseased tissues in the body (such as tumors) without exposing or tearing the skin or causing tissue damage. Either ultrasound or MRI is used to identify and target the tissue being treated and direct and monitor therapy in real-time and show its effectiveness. The FDA currently approves HIFU to treat uterine fibroids, pain relief for bone metastasis, and prostate ablation for more recent years. HIFU is also tested for wound closure and bleeding, the breaking up of blood clots, and the temporary opening of the blood-brain barrier to the passage of medications.

2.3. Aneurysm

An aneurysm is a disease that causes the enlargement of an artery. It is due to the prolonged high blood pressure and the high elasticity in the wall of the artery. There are usually no symptoms associated with this disease. However, long-term aneurysm can be fatal and dangerous and leads to life-threatening internal bleeding. According to statistics from the disease control and prevention centers, the death rate caused by aortic aneurysms in the united states annually is over 25,000. Aneurysm affects different arteries, but the main arteries mostly affected by this are the brain's arteries and heart. One type of aneurysm, aortic aneurysm, damages the body's main artery, causing internal bleeding. Smoking and high blood pressure have considered the main factors that play an essential role in developing this

disease. The possibility of having an aneurysm varies between individuals such as smokers, and individuals having hypertension are at high risk of developing this disease. Occasionally, this can be very serious that it may need surgical treatment to prevent artery rupture and operated by surgeons only if they are fatal [15].

2.3.1. Types of aneurysms

There are various types of aneurysms, and they are classified based on location in which these are located. The two most common locations for an aneurysm are the arteries of the brain and heart. There are two shapes of swelling in the artery having aneurysms:

- Fusiform aneurysms swelling are present on all sides of the vessels.

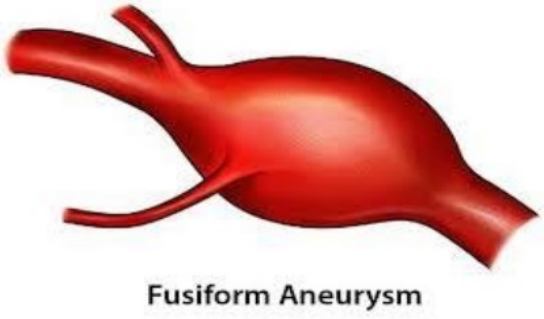

Figure 15: Fusiform aneurysms vessel [16]

- Saccular aneurysms swelling or bulge are present on one side of the vessels.

Figure 16: saccular aneurysms vessel [17]

The size of the swelling or bulge describes the risk of rupture caused by the aneurysms.

2.3.2. Aortic aneurysm

An artery that starts from the heart's left ventricle and passes through the chest and the abdominal cavities is referred to as the aorta. Usually, an aorta is about 2 to 3 cm, but in the case of aneurysms, a bulge increase around 5cm in diameter. The most common type of aorta aneurysm in the abdominal portion of the aorta is the abdomen's aneurysm (AAA). The survival rate without surgery in the case of AAA over 6cm in diameter is 20%. But if it is treated surgically at the proper time, it has a survival ratio of about 50%. Another type of aneurysm, thoracic aortic aneurysm (TAA), is significantly less common as it only occurs at a rate of 25%. It can affect the aorta that runs through the chest. In this case, the survival rate without treatment, is about 56% and 85% in the subject or timely surgery [18].

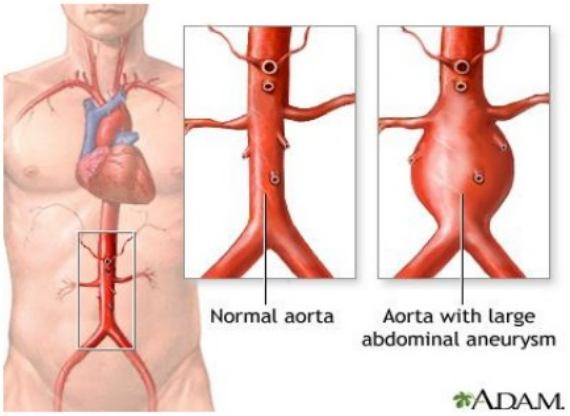

Figure 17: Aortic aneurysm [19]

Figure 18: Aortic aneurysm (ultrasonic view) [20]

2.3.3. Cerebral aneurysm

Intracranial aneurysms, also are known as berry aneurysms, are the arteries that supply blood to the brain. 40% of Intracranial aneurysms can be fatal and caused death within 24 hours 66% of patients who survive this condition experience neurological disability. Subarachnoid hemorrhage (SAH) is the most common type caused by ruptured cerebral aneurysms [21].

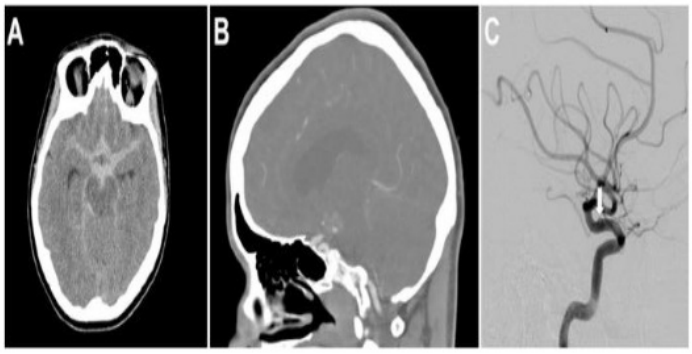

Figure 19: Cerebral aneurysm (ultrasonic view) [22]

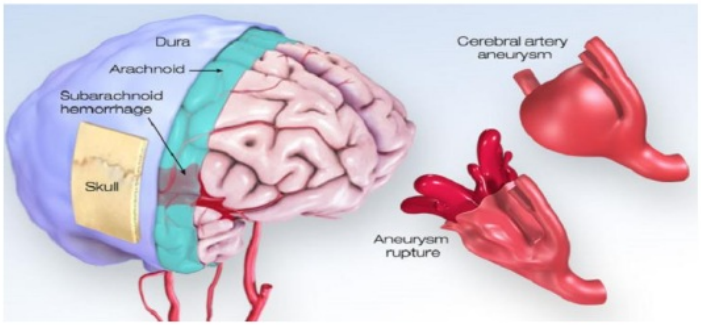

Figure 20: Cerebral aneurysm [23]

2.3.4. Peripheral aneurysm

An aneurysm that occurs in the peripheral artery is called a peripheral aneurysm. It has less chance to rupture than aortic aneurysms. It is further divided into the popliteal aneurysm (this most common type of peripheral aneurysm cause bulge behind the knee), splenic aneurysm of the artery (this peripheral aneurysm takes place in the spleen), mesente

ric ane--urysm of the artery, and femoral aneurysm of the artery (this type of peripheral aneurysm affects the femoral artery present in the groin) [24].

Figure 21: Peripheral aneurysm artery [25]

Figure 22: Peripheral aneurysm artery (ultrasonic view) [26]

2.4. Treatment

All unruptured aneurysms have not actively required treatment, but emergency surgery is needed under certain conditions of aneurysms. If symptoms are not obvious, surgeons m onitor an unruptured aortic aneurysm. Medication is part of conventional management, or they may go with active surgical treatment. Medical surgery is needed for a ruptured aneurysm because if not performed, it can be fatal. Certain factors are considered before surgery of an unruptured aneurysm that depends on the patients' condition and the aneurysm's features. Factors are age, health condition, coexisting conditions, patient choice, the size of

aneurysm, location in body, and growth rate. A rapidly growing aortic surgery aneurysm has immediately required surgery, consisting of two types, such as open surgery. In this case, a large cut is made in the abdomen for aorta exposure, and for repairing, a graft is then applied to endovascular stent surgery. In endovascular stent surgery, a small incision through the lip is accessed for blood vessels by doctors, and the insertion of endovascular graft is inserted through a catheter. For the sealing of the aorta, the graft is positioned. The following are some risks in endovascular surgery: blood leakage around the graft, bleeding during the surgery, stent blockage, nerve damage, sometimes resulting in fatigue and pain in legs [27]. Erectile dysfunction is usually referred to as the unsuccessful surgery that requires a further operation slippage of the stent conditions like bleeding around the graft will need another surgery.

*2.4.1. **Cerebral aneurysm treatment options***

Emergency surgery is required in case of a ruptured intracerebral aneurysm. But surgery is performed if there is high risk of rupture in a brain aneurysm because the risk of surgical complications is very high. The dependence of rupture in the case of AAA depends on the rupture's size and location. Patients are advised to monitor the risk factor for a brain aneurysm, such as checking their blood pressure. Surgery is preferred if subarachnoid bleed ing results in the case of a ruptured cranial aneurysm and refer to a medical emergency. This surgery is performed to close ruptured artery to stop bleeding [28].

2.5. Types of biosensors

The various types of biosensors are categorized according to the sensor system, and the biological content in the literature are listed below.

Cooper and Singleton (2007) analyzed biosensors' widespread exploitation in molecular recognition analysis based on surface plasmon resonance (SPR). They explored binding properties, affinity, kinetics, and conformation changes in connection with molecular recognition events and, more recently, platforms based on piezoelectric acoustic sensors, mainly (BAW) is called "bulk acoustic wave", "thickness shear mode" (TSM). They highlighted the theoretical and functional aspects of acoustic analysis technology and Tiny

molecular weight ligands, enzymes, proteins, nuclear acids, viruses, bacteria, cells, and lipid and polymer interfaces are the major application fields [29].

Suet al. (2010) investigated the production and application of amperometric, potentiometry, conductometry, voltammetry, microbial fuel cell, fluorescence, bioluminescence, and calorimetric microbial biosensors in recent years. They explored the use of microbial biosensors for environmental, food, and biomedical applications. Furthermore, future strategies to design microbial biosensors are also discussed [30].

Roda et al. (2011) researched a compact biosensor focused on the genetically modified bioluminescent (BL) cells using genetic basics. On a 4/3 multiwall cartridge, cells were immobilized by a new biocompatible matrix, which preserved their vitality. The cartridge has been placed in close contact with a cooled CCD sensor using a fiber optic taper to image and measure the BL signal. Genetic modification to express recognition-elements with the analyte's association led to luciferase-expression modified to yeast and bacterial cells using a reporter gene-technology. 3 biosensors have been developed. The 1st detects androgenic compounds with green-emitting yeast cells. The human androgen receptor and the red mutant of the same genus regulate pyralis luciferase. The 2nd biosensor identifies two types of compounds with yeast strains bred to release mutant androgens or estrogenic mutations arising from firefly luciferases. The third biosensor senses iso-propyl-d-1-thio-galacto-pyranoside lactose analog using two E. One-piece uses the lake operon as an identification factor for p. Pyralis luciferase expression. The other piece is used to regulate Gaussia princeps luciferase's vitality, which needs a different luciferin substratum. The cells remained stable for upto one month. The measurement can be identified with fair sensitivity and precision at nanomolar levels if inner vitality regulation corrects the particular signal [31].

Koydemir et al. (2011) introduced traditional approaches, microfluid biosensors, and commercial products to detect methicillin-resistant Staphylococcus aureus (MRSA) is one of the most significant challenges to nosocomial infections in many parts of the world. Early detection of MRSA in patient specimens is essential in managing control measures in medical units, providing adequate care, reducing morbidity, and mortality. Therefore, high sensitivity and specificity quick and low-cost diagnostic systems are crucial to avoid MRSA

is an emerging threat to public health. The design and manufacturing of modern diagnostic systems involve cooperation among various disciplines to create new clinical diagnostic challenges and satisfy clinicians' demands. It was certain that MEMS and nanotechnology-based detection methods would take current techniques in clinical diagnosis soon. The estimation of new trends for specificity, sensitivity, cost-effectiveness, disability, low weight, ease of use, and facile access should be considered [32].

Perumal and Hashim (2013) examined the ability to detect molecules related to the body's pathology and physiology with the perfection of sensitivity and specificity. It was a tremendous effort in the early diagnosis and treatment of diseases that can significantly reduce patient care costs associated with the advanced stages of many diseases. On the other hand, these techniques have many potential limitations in patient response and cost-effectiveness. They researched that a phytochemical transducer that transforms this recognition into a visible output signal can be coupled to biosensors. Over the past few years, they have examined some of the key developments in this area, analyzed the application opportunities and addressed the difficulties, methods and obstacles to promote wider interest in developing the biosensors and enhancing the applications for medical diagnoses [33].

An arterial pulse controlled by Park et al. (2017) using an epidermal pressure sensor is an essential technology for detecting cardiovascular disease's early occurrence and determining personal health. A self-powered piezoelectric pulse sensor causes radial pulse signals in near-surface arteries to be measured in vivo. The inorganic piezoelectric sensor on the ultra-thin plastic includes the rough skin's complicated structure, allowing it to respond to the slight pulse changes on the skin's surface. Experimental tests include sensitivity (ca. 0.018 kPa−1), reaction time (ca. 60 ms), and the sensor's strong mechanical reliability. Wireless transfer of sensed arterial pressure signals to a mobile phone indicates the likelihood of an integrated pulse tracking device even in real-time [34].

Fan et al. (2008) analyzed the recent development in using the mark-free protocol to identify unlabeled or unmodified biomolecules and their natural states. The emphasis was on optical biosensors used as the sensing transduction signal to adjust the refractive index. Several optical, label-free biosensing systems were offered to comprise Plasmon resonance, interferometers, maps, fiber gratings, ring resonators, and photonic crystals [35].

2.6. Ultrasound biosensor

Ultrasound can easily visualize deep tissue with a high resolution but does not have the biosensors required to link its contrast to real biomolecular activity, such as enzymes. The first acoustic biosensors are implemented to address this constraint molecules' lighting up' in ultrasound images in response to protease action. These biosensors focus on a unique class of air-filled protein nanostructures gas vesicles.

Practically any biological mechanism in living organisms requires complex changes in individual molecules' concentration or behavior. Visualizing these improvements inside the preserved living tissue is important for understanding the next millennium's biological process and medicines. A broad range of genetically encoded fluorescent sensors has been created from images of particular molecular and cellular events. Therefore, the use of such biosensors in living organisms is difficult because of the restricted penetration of light into tissue.

2.6.1. Acoustic wave devices

The direct radiation force used by Kuznetsova and Coakley (2006) moves the deferred particles & concentrates them into acoustic node planes, smoothly moving cells to small analytical separators. The DRF results were analyzed, which significantly improved the latex-agglutination test's sensitivity by concentrating particles in the analytical sample in node position, thereby significantly raising the rate of the encounter between antibody and antigens. Direct radiation force & acoustic streaming provided the significant impact of the ultrasonic standing wave at surface particle action (USW). They captured biotinylated particles and spores in one-fourth wavelength USW resonator on a coated acoustic reflector with 70-fold and 100-fold DRF enhanced than the situation in the absence of ultrasound. Acoustics preparation for mixing small analytical samples was successfully used. Mixing, DNA hybridization, & the capture efficiency of Escherichia coli K12 on the surface of immunomagnetic beads significantly increase micro capital streaming. The acoustic streaming induced by immuno-sensors of the longitudinal standing wave and flexural plates increases the antigen detection 5 or 3 times. The combined DRF and acoustic streaming effects have increased reaction rate between cell and retroviral suspended mix [37].

Länge et al. (2008) a summary of 20 years of foreign biosensors has been discussed. Implementation based on specific surface acoustic wave types (SAW), which allow the detection of highly sensitive bio-relevance In liquid media, molecules (like water and aqueous as buffer results). In 1987 first approaches were made to either use horizontally polarized shear waves (HPSW) with delayed lithium tantalate (LiTaO3) substrates or quartz SAW resonator structures LiTaO3 with standard gratings for mass. Supposed to be named “surface transverse waves" (STW) And when operated in liquids, they have relatively low attenuation values. Later on, love wave Devices have been built To reduce attenuation dramatically, it used a film resonance effect. The creation of suitable films followed all these sensory approaches. Initially, superficial layers ware used to adsorbed the antibodies. Later methods used different types of covalent layers, such as intermediate hydrogel layers. The Latest methods include integrating SAW biosensors into compact systems with combined sample management fluid. In micromachine polymer boxes, the SAW biosensors can be integrated. The device can be expanded to build flexible biosensor arrays for general laboratory use or diagnostic purposes by combining these two functions [38].

For many decades, Fogel et al. (2016) have studied resonator and acoustic wave devices used in gravimetric sensing for various biological and chemical studies. devices are work combining the measurement and (e.g., analyte adsorption) as Modulation of the physical properties of the acoustic wave (e.g., resonant frequency, acoustic velocity, or dissipation) that could be correlated with the volume of analyte adsorbed. These devices can also be miniatured, with cost, size, and scalability advantages and potential extra features including integration with microfluidics and electronics, smaller size sensibilities and higher operating frequencies, and ability to multiplex detect hundreds of devices embedded in a single chip, and increased throat. Furthermore, the production of devices is also consistent with semiconductor batch production techniques, which allow the production process to be inexpensive, scalable, and have a high degree of precision and reproductivity. Integration with microfluidics' handling often allows sufficient sample preprocessing/cleansing/amplifi cation measures to boost selectivity and overall signal to noise ratio [39].

2.6.2. MEMS-based sensors

Grayson et al. (2003) manufactured MEMS devices to develop integrated circuits using similar microfabrication techniques. However, they also have moving components that allow the system to perform physical or analytical functions. Though MEMS can be aseptically manufactured and hermetically sealed, the component material's biocompatibility is crucial for MEMS in vivo. MEMS interest in biological applications grows rapidly, and opportunities for biosensors, pacemakers, vaccine capsules, and drug delivery have been growing. The key to all of these applications is to use MEMS unique features, such as sensitivity to the analyte, electrical reaction, time control, cells, and organelle-like functionality, for optimum effect. This paper deals with enhancing MEMS's biological integration and other implantable devices by applying micro-manufacturing technologies and concepts. Innovative methods are tested for enhanced physical and chemical system integration in the body. The untapped potential of MEMS may lie with the actuation of the nervous and endocrine systems. MEMS' ability to supply potent drugs or hormones and specific temporal controls will provide new therapies for these systems disorders [40].

Voiculescu and Nordin (2011) concluded that MEMS devices based on acoustic waves provide an exciting technology platform for developing responsive, compact, real-time bio-sensors. MEMS acoustic wave-based biosensor manufacturing facilitates chip thinning, power consumption reduction, and electronic circuit integration. The biosensors are incorporated in a microfluidic device for biological applications, and the sensing region is enclosed in a biospecific layer. As the analyst interacts with the sensing layer, changes in the biospecific layer's mass and viscosity can be detected by measuring acoustic wave proprietary changes such as speed, attenuation, resonant frequency, and time delay. Some acoustic wave devices without a significant quality factor could be incorporated into microfluidic systems. Acoustic wave-based MEMS devices identified as biosensors in the literature, and presented in this analysis are film bulk acoustic wave resonators (FBAR), SAW resonators. Various approaches for FBARs, SAW resonators, and SAW delay lines are proposed for multiple biochemical applications [41].

Multiple ultrasonic biosensors have been previously developed for a variety of applications. However, to the best of our knowledge, the device presented in this thesis is the first ultrasonic transducer that is designed for on-skin use to detect arterial rupture.

SIMULATIONS

3.1. Background of piezoelectric transducers

The transducer integrates a piezoelectric element converting mechanical vibrations in electrical signals into mechanical vibrations and electrical signals (receive mode). A transducer's Many variables affect the actions, mechanical and electrical architecture, including material, condition is based on an external mechanical and electrical load. Parameters like radiation surface area, mechanical damping, accommodation, connector, and other physical construction variables are used in mechanical construction. When designing two transducers that have similar performance features, transducer manufacturers are hard-pressed.

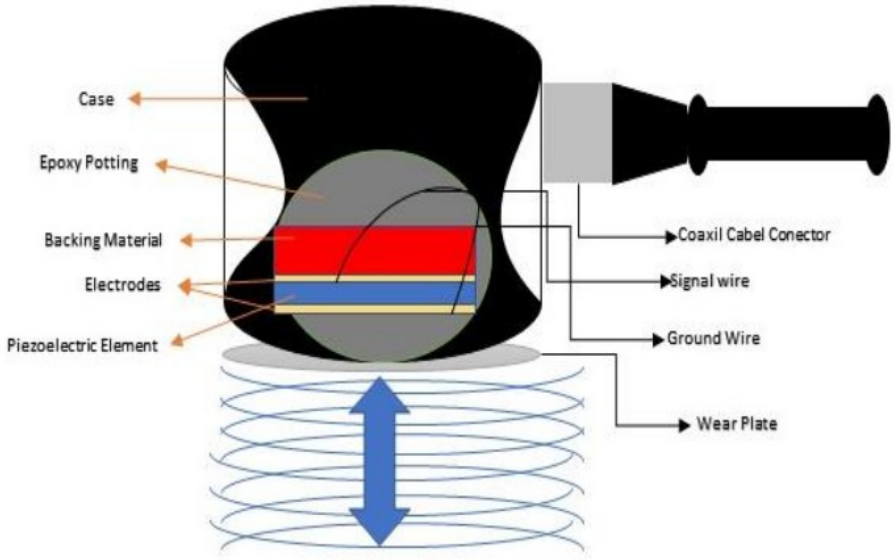

Figure 23:Typical contact transducer

A distinctive contact transducer cut is shown above. As explained before, the piezoelectric part was cut to half the desired wavelength. An impedance match is put between the active part and the transducer's face. Optimum impedance matching is accomplished by slicing the

matching layer into quarter the desired wavelength. This wavelength holds waves mirrored in the in a phase of matching layer after that they leaving the layer. Transducers often add wear plate to shield the corresponding layer from scratch.

3.1.1. Bandwidth, Frequency and Transducer Efficiency

Many of the transducers are manufactured to be an efficient transmitter, and others to be more efficient receiver. The transducer performing well in one application will not always yield the desired results in another application. E.g., sensitivity to the small defects is proportional to the transducer's efficiency as a transmitter & receiver product. The resolution, the ability to detect defects in the material near the proximity or surface, requires highly damped transducer.

The definition of bandwidth, or frequency range, connected with a transducer is also important to understand. The central or middle frequency is the frequency noted on a transducer and mainly depends on backing material. The highly damped transducers will react to frequencies below and above the central frequency. The widespread frequency range provides high-resolution power for the transducer. Weaker resolving power and a narrower frequency range. But greater penetration, will be seen by less damped transducers. The central frequency will also specify a transducer's capabilities. Lower frequencies have greater energy and penetration into a material (0.5MHz-2.25MHz). Although high-frequency crystals (15.0MHz-25.0MHz) offer decreased penetration, tiny discontinuities are more sensitive. When used with proper instrumentation, high-frequency transducers will significantly increase thickness measurement capabilities and flaw resolution. Broadband transducers upto 150mhz are commercially viable.

Transducers are designed to withstand the assault but should be managed carefully. Misuse, like falling, can cause cracking of wear plate, part, or back material. Damage to a transducer is also noted on the A-scan presentation as an initial pulse enlargement.

3.1.2. Resonant frequency

A resonant frequency is an object's natural vibrating frequency, usually referred to as an f with a subscription zero (f_o). This type of resonance is observed when an object is in equilibrium with acting forces and could vibrate long under perfect conditions.

Formula:

$$f_o = \frac{1}{\pi}\sqrt{k/m} \qquad (2)$$

Find spring resonance frequency, the letter "m" is the spring-mass, while "k" is the spring constant that can be given in a problem. By using the formula v = λf to find a single continuous wave's resonance frequency. The letter "v" refers to wave velocity, while "λ" denotes wavelength size. This formula states that wave velocity equals wavelength distance calculated by resonance frequency. In manipulating this equation, resonance frequency equals wave velocity divided by wavelength distance [42].

3.1.3. Ultrasonic Near-Field and Far-Field Areas

Both far-field and near-field areas are included in an ultrasonic transducer beam of ultrasound emitted. Due to the wave interference, the sound pressure near wave source fluctuates sharply, and a set of minimum and maximum sound pressure appears, which is cylindrical. The sound pressure is not regular at this point, and the ultrasonic-propagation is unpredictable. The distance b/w maximum value of the sound source & the last sound pressure is called the near field duration, represented by N. The near-field area is called the area within N. The area where the distance is greater than length of near-field region from axis of the wave source to wave source is divergent & is called the far-field region. In figure 24, a sound field diagram is shown. An equation can determine the near-field ultrasonic region.

$$N = \frac{D^2}{4\lambda} \qquad (3)$$

D is the ultrasonic sensor diameter, and λ is wavelength of ultrasonic wave propagation in medium, which can be calculated using the following equation.

$$\lambda = \frac{c}{f} \qquad (4)$$

C is wave velocity of ultrasonic wave propagation in the medium, f, and m/s is the Hz ultrasonic frequency. Hence, the near-field length of beam of ultrasound is related to the frequency of the medium's ultrasound propagation and diameter (area) of the piezoelectric plate and the speed. At a certain speed & frequency, the bigger the diameter is, the longer near-field length will be.[43]

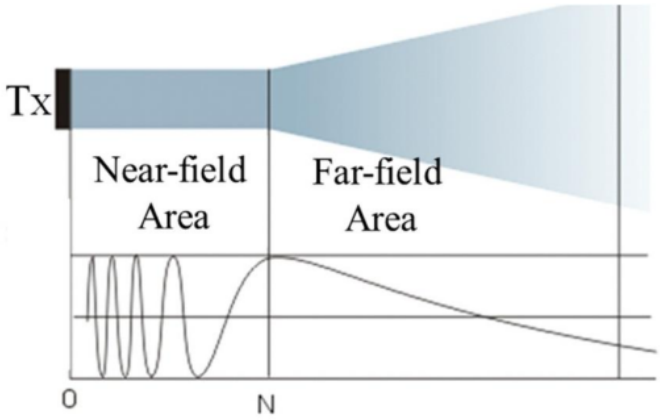

Figure 24: Sound field diagram

Wanjia Gao et al., 2020, described the variables influencing the duration of the near-field ultrasonic. Propose the optimum length of buffer block and minimum length to avoid near field. Evaluations show that when ultrasonic probe parameters are 15 millimeters in diameter, 1 MHz in frequency, & ±15 V in ultrasonic wave amplitude emitted, the best results are found, when length of the buffer-block is 22 millimeters. When probe's diameter is 10 millimeters, the buffer block's size should be approximately 5 mm to ensure the measured results' validity. When using ultrasonics to calculate the liquid level, this research will effectively avoid blind region of emitted waves. It provides an important basis for ultrasonic probe selection & design [44].

Franco et al.,2011, present the model according to the acoustic field radiated by ultrasonic transducers and arrays. The impulse response of the velocity potential and the discrete representation methods were used. The first approach deals with estimating the exact impulse response, in which only basic geometries, such as the circular piston, can provide

solutions. The second method is an approximate solution based on discretization in small elementary areas of the acoustic aperture, each of which radiates a spherical wave. By Using a scanning device, the experimental results were collected. A 3.5 MHz array of 16 elements all submerged in water, the acoustic field radiated from a 1 MHz circular transducer was measured. The acoustic field emitted by the array was simulated and measured, emphasizing a 30 mm radius with 0° and 20° deflections [45].

Anthony Gachagan et al. describes creating a flexible piezoelectric transducer in plate-like structures for the generation and detection of ultrasonic symmetrical Lamb waves. This piezoplatele transducer's structure consists of a series of miniature piezoceramic plates embedded in a soft-setting polymer filler material, combining the active piezoceramic process's efficiency a degree of flexibility that is a function of the dimensions of the platelet/polymer. The piezoplatelet transducer structure's efficiency was evaluated using a combination of linear systems and finite-element modeling for several condition-monitoring applications, assisted by experimental results. Importantly, the transducer, each operating in the thickness mode and well decoupled from neighboring piezoelectric components, is shown to act as an ensemble of platelets. A unimodal s1 Lamb wave, at 1.45 MHz, was produced and detected in a 3-mm thick steel plate using this transducer configuration. A propagation distance of nearly 1 m was observed on a fiber-reinforced composite plate for s0 Lamb wave generation/detection [46].

Jan Kredba and Miroslav Holada present one way for a single piezoelectric ultrasonic sensor to measure distances between multiple objects with the high precision method. The digital signal processing described in this paper is mainly based on digital filtering and a combination of cross-correlation and phase-shifting methods. Only one piezoelectric transducer was used to transmit and receive ultrasonic waves. The impedance matching circuit for the piezoelectric transducer was designed to increase the signal ratio to noise and improve measurement accuracy. These obtained signal processing methodologies enabled the use of low-cost piezoelectric transducers with a resonant frequency of 40 kHz to measure multiple object distances with a resolution of 1 mm over 3 m [47].

3.2. COMSOL Software

COMSOL multiphysics aims to build models and simulations based on physics. The model builder enables the combination of multiple physics models in any order for simulations of a real-world phenomenon. The COMSOL provides a range of tools to build simulations. COMSOL multiphysics helps the user to communicate with traditional physics-based systems and partial differential equation systems (PDEs). For electrical, mechanical, fluid, acoustic, and chemical applications, COMSOL offers IDE and a single workflow. An ultrasonic biosensor for detecting arterial rupture was simulated by COMSOL multiphysics in this work.

3.3. Parameters

Parameters are used to describe specific modeled object characteristics. A parameter is usually a constant value in a simulation and is adjusted when modifying the model's behavior. The following table shows the parameters used in the proposed model. Amplitude is the value of the applied sound pressure, and frequency is the frequency of the pressure signal. The simulation step is the step value to control time, and simulation time is the process's total duration. Moreover, skin speed of sound is the value of the sound speed in human skin or tissue.

Table 1: Parameters

Name	Expression	Description
Amplitude	10	10
Period	0.5	0.5
Frequency	1000000	$1E^{7}$
simulation step	1/(100*frequency)	$5E^{-9}$
Simulation time	500/frequency	$1E^{-5}$

Skin Speed of sound	1540	1540

3.4. Geometry

The COMSOL has different geometry models such as 2D, 3D, 1D axisymmetric, and 2D axisymmetric. This simulation uses a 2D model with different geometric operations to build an ultrasonic biosensor model. The used values of the model are given in the following table.

Table 2: geometry values

Rectangle	Size and Shape		Position (base corner)	
No	Width (mm)	Height (mm)	X Axis	Y Axis
skin(r1)	10	10	0	12
Artery(r2)	10	1	0	11
Blood Part(r3)	10	5	0	6
Artery(r4)	10	1	0	5
Skin2(r5)	10	5	0	0
Point1(pt1)	-	-	4.9	22
Point2(pt2)	-	-	5.1	22

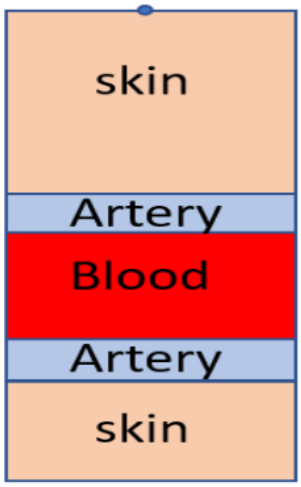

Figure 25: 2D geometry model

3.5. Materials

In this model, multiple materials are used, such as skin, blood, and artery. Each material includes some physical properties with the values or functions describing the material. As the skin is used in the proposed model, the human body is included in the COMSOL simulation. Different skin parameters are used, such as skin, diameter, and domain. The thickness of the skin is 10mm, the diameter is 10mm, and the domain is 1 and 5. Other skin properties are shown in table 3. Further, the addition of some blank material is used for blood and artery. In the model, the blood section is in the third domain. The parameters used in the blood module are given in table 3. Moreover, the artery domain is illustrated in the 2nd and 4th sections of figure 26, and materials used for this section are given below.

3.5.1. Properties of materials

Different materials properties used in the model are described in this section, such as Poisons ratio, Young modulus, mass density, and sound speed. In solid mechanics, Poisson's ratio (υ) is a measure of the Poisson effect, the phenomenon in which a material tends to expand in directions perpendicular to the direction of compression. The Poisson effect in skin, blood, and artery. The value of Poisson's ratio is the negative of the ratio of transverse

strain to axial strain. The young's modulus (E or Y) measures a solid's stiffness or resistance to elastic deformation under load. It relates stress (force per unit area) to strain (proportional deformation) along an axis or line. The mass density of an object is defined as its mass per unit volume. This parameter can be expressed using several different units, including kilograms per meter cubed (kg/m^3). Mass density represents the amount of mass (or the number of particles) of a substance, material, or object related to the space it occupies. The speed of sound is the distance travelled by a sound wave per unit of time as it propagates across an elastic medium. At 20°C (68°F), sound in air is around 343 meters per second.

Table 3: Material properties

Skin Material content (Properties)			
Property	Variable	Value	Unit
Mass Density	P	1109	Kg/m^3
Speed of sound	C	1504	m/s
Blood Material content (Properties)			
Poisons Ratio	Y	0.49	I
Youngs Modulus	E	2e4	Pa
Mass density	P	1160	Kg/m^3
Speed of sound	C	1450	m/s
Artery Material Content (Properties)			
Poisons Ratio	Y	0.45	I
Youngs Modulus	E	2e5	Pa

Mass density	P	1160	Kg/m^3

3.6. Physics

There are multiple physical interfaces available for use, such as acoustic, electrochemical, radiofrequency, semiconductor, etc. There are also different ways of accessing the physical interfaces and adding a model. In this model, pressure acoustic, transient (actd) are used

3.6.1. Pressure acoustics, transient (actd)

The transient (actd) acoustics measure the pressure difference when modeling acoustic waves' propagation in fluids under a quiet background. It is ideal for time-based simulations with arbitrary fields and sources that are dependent on time. Table 4 shows the pressure acoustics domain and pressure acoustics equation. The equations for mainly time-dependent simulation of (transient) acoustics. The scalar wave equation in which p_t is the overall acoustic pressure, ρ is the mass density, c is the sound velocity, q_d is the source of the dipole domain, and Q_m is the source of the monopole domain. The speed of sound and density can depend on space in this wave equation formulation, but it only varies slowly in time, at a time scale much slower than the variations in the acoustic signal. Following figure 24 illustrates the pressure acoustics, transient in the proposed model.

Table 4: Pressure acoustics domain

Domain	1,3,5
Equation	Equation from (Time-Dependent)
Study Controlled	Study1, Time-Dependent

Equation (5)	$\frac{1}{pc2}\frac{\partial^2 pt}{\partial^2 t} + \nabla.\left(-\frac{1}{p}\nabla p_t - q_d\right) = Q_m$ $pt = p2 + pb$

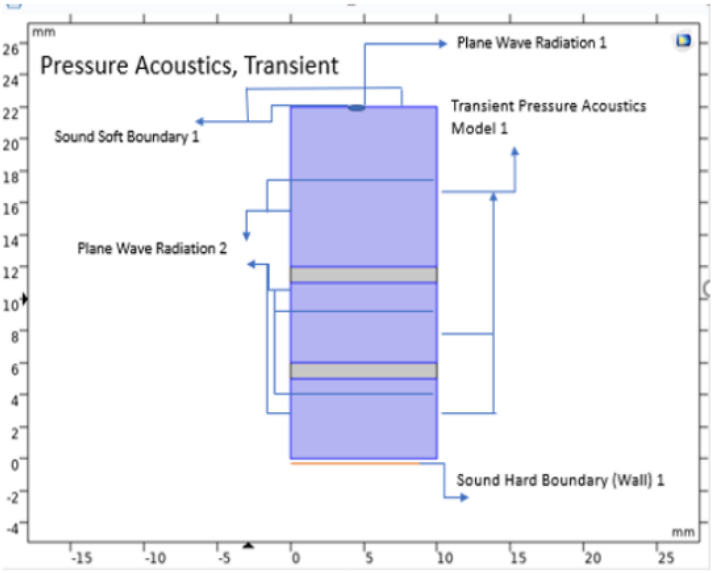

Figure 26: pressure acoustics, transient

3.6.1.1. ***Features***

- Transient pressure acoustics model 1
- Sound hard boundary (Wall) 1
- Initial values 1
- Plane-wave radiation 1
- Plane-wave radiation 2

3.6.1.2. Model 1 is for Transient pressure acoustics.

The model node for transient pressure acoustics adds the acoustic equations, mainly time-dependent. The transient pressure acoustics model 1 uses two different materials: Skin

speed of sound and blood speed of sound. Moreover, the values of skin mass density and blood mass density are shown in the table below.

Table 5:The transient pressure acoustics model detail

Speed of sound	C	[From material]	Skin	1540 m/s
			Blood	1570 m/s
Mass Density	P	[From material]	Skin	1190 kg/m^3
			Blood	1060 kg/m^3

3.6.1.3. Sound hard boundary

The sound hard boundary controls the state condition of model hard boundary surfaces or walls, A boundary at which the common acceleration part (the velocity) is going to be zero , equation shown in table 6. For zero dipole domain source ($q_d = 0$) and constant fluid density ρc, the normal derivative of the pressure is zero at the boundary. Table 6 shows the boundary of the model.

Boundary	2
Equation (Study 1, Time-Dependent) (6)	$-\boldsymbol{n} \cdot \left(-\frac{1}{\rho}(\nabla \boldsymbol{p_t} - \boldsymbol{q_d}\right) = \mathbf{0}$

Table 6: Sound hard boundary

3.6.1.4. Initial Values

The Initial Values node adds an initial pressure value. An initial value for the pressure time derivative is also applied in the time domain. For a nonlinear solver, the initial values may serve as an initial guess or characterize the initial state that will then develop with time. Table 7 shows the initial value of domain, initial values for the Pressure p (SI unit: Pa), and first-time derivative $\partial p/\partial t$ (SI unit: Pa/s). The below table also shows the plane wave radiation boundary.

Table 7:initial values domain's and plane wave radiation boundary

Domain	2
Initial Values	Pressure (P=0 pa)
Pressure, the first-time derivative	$\partial p^2 / \partial t$ (0) pa/s
plane wave radiation	
Boundary	12

3.6.1.5. Incident Pressure field 1

To perform a plane wave expansion, the incident pressure field has incorporated features. The incident pressure field pi is a pre-defined plane wave, user-defined pressure field type, and the incident pressure boundary. Moreover, the plane-wave radiation boundaries are given in the table below.

Table 8: Incident pressure field and plane-wave radiation 2

Incident Pressure Field	
Pressure field type	User-Defined

Boundary	12
Pi	A*sin(-2*pi*f*y/skinspeedofsound-2*pi*f*t) * (t<=(period/f))
Plane-wave Radiation 2	
Boundary	1,5,9,14,16,18

3.7. Multiphysics

Multiphysics is defined as a coupled modeling approach of studies that demand simultaneous addressing of so far separate physical disciplines and combining them to generate relational mathematical models and validate them with controlled experiments to enhance the understanding of natural behavior. This section describes the physics involved in the coupling of multi-physics. Table 11 shows acoustic-structure boundaries coupled interfaces in multi-physics. Figure 27 illustrates the acoustic-structure boundary.

Table 9:Boundary of Multiphysics

Boundary	4,6,8,10
Acoustic-structure Boundary 1	(asb)1
Couple interfaces	Pressure Acoustics

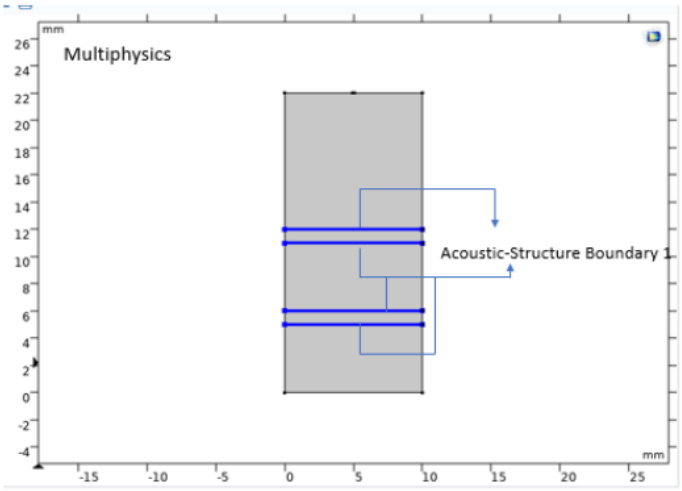

Figure 27: Acoustic-structure boundary

3.8. Mesh1

This proposed model used physics-controlled mesh by design, which is based on the unstirred tetrahedral mesh. This mesh is automatically generated and adjusted to the device's physics setting, with the unit size default to a standard. The mashing process is invisible, consisting of a scale and a free tetrahedral node. This simulation is using some manual mash sizes (element size parameter), shown below in table 12, and figure 28 shows the model mash.

Table 10:Mesh size values

Maximum element size	0.25 (mm)
Minimum element size	0.00165 (mm)
The maximum element growth rate	2
Curvature factor	0.25
Resolution of narrow regions	1

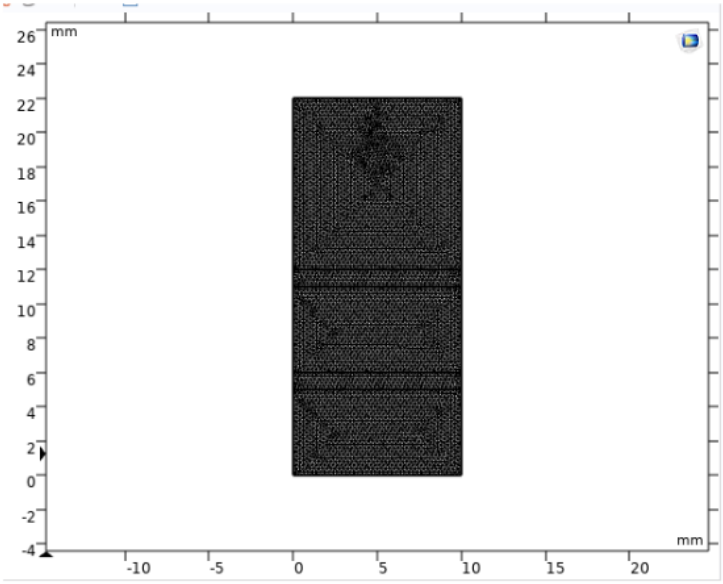

Figure 28: Mesh

3.9. Study 1

The equations and physics interfaces included in the computation and mesh selection are controlled by study steps. This simulation uses a time-dependent model study that computes the model's frequencies and model response. Table 13 shows the time-dependent study.

Table 11: Time-dependent study.

Time (Unit)	(S)
Start (time)	0
Step (time)	$1E^{-9}$
Stop (time)	$5E^{-5}$

3.10. Results

This section, illustrates the results of proposed model. The results are divided into two sections that are given in the COMSOL.

3.10.1. ***Acoustic pressure (actd)***

Acoustic pressure is the local pressure deviation from the ambient (average, or equilibrium) atmospheric pressure caused by a sound wave. The (SI) unit of sound pressure is the pascal (Pa). Figure 29 illustrates the total acoustic pressure field (actd) for 10MHz in the proposed model. The figure below shows the 10 MHz frequency acoustic pressure field. Figure 29a shows the signal is coming towards the artery, and figure 29b shows the signal after hitting the artery. Afterward, figure 29c illustrates the signal returning to the sensor. This process continues until the user-selected time duration is finished.

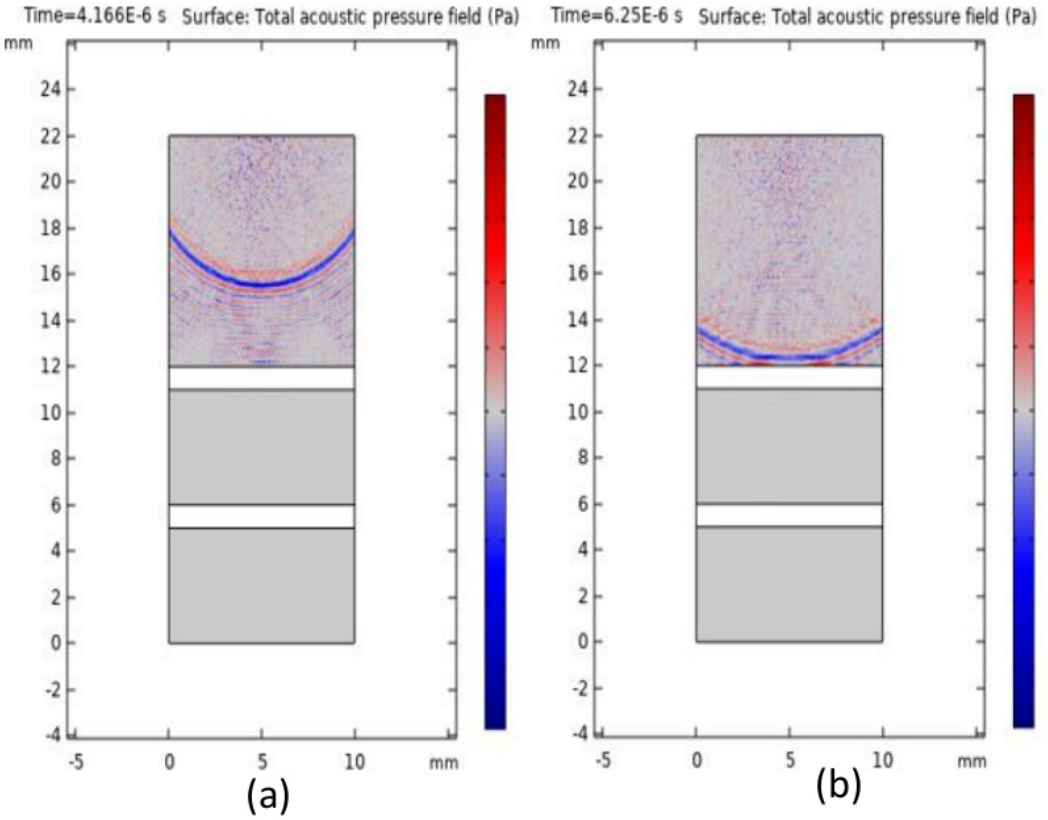

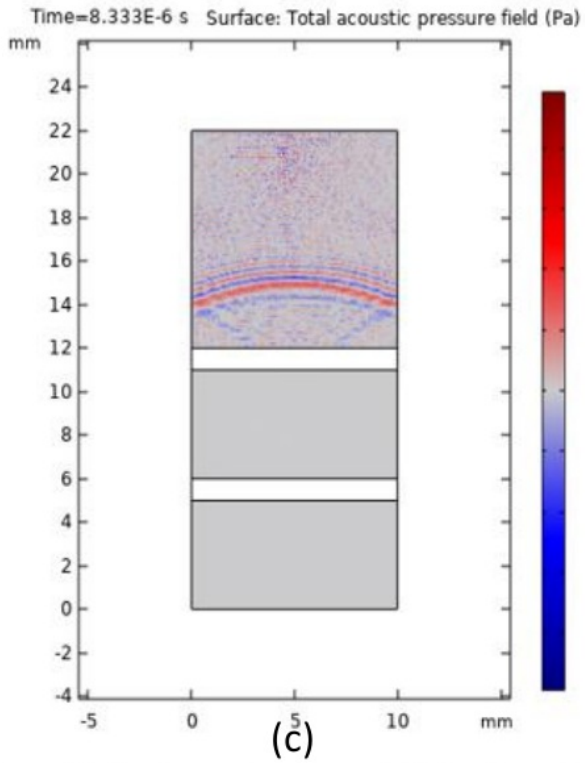

(c)

Figure 29:Total acoustic pressure field (actd) graphics

*3.10.2. **Von Mises stress***

The von Mises stress is used to predict materials yielding under any loading condition resulting from simple uniaxial tensile tests. Figure 28 indicates the stress imposed by the wave after hitting the material in the proposed model.

A 1D cross-section point plot displays a quantity at one or more points in time, with a parameter range. In this model, the data step has a cut point (2D1) and time selection (All); Figure 31 illustrates the COMSOL spectrum results for 10MHz in the proposed model.

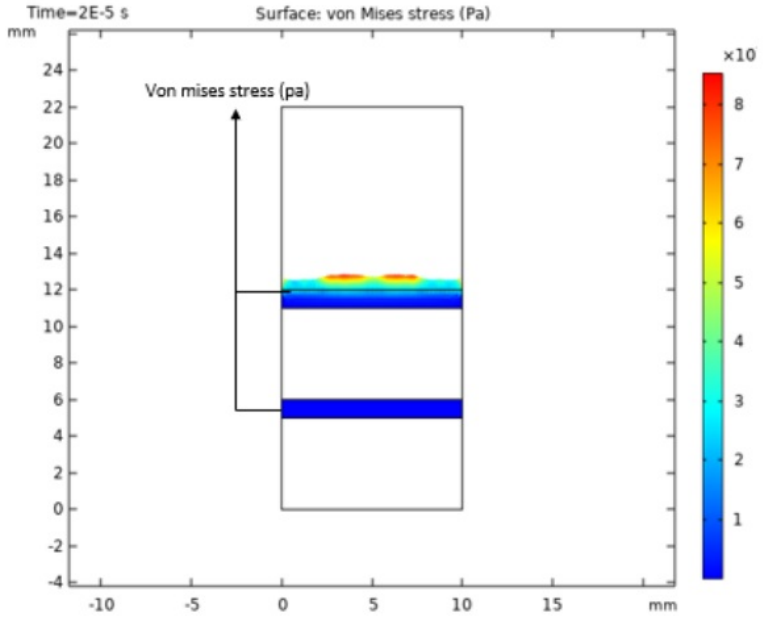

Figure 30: Von mises stress (pa) graphics

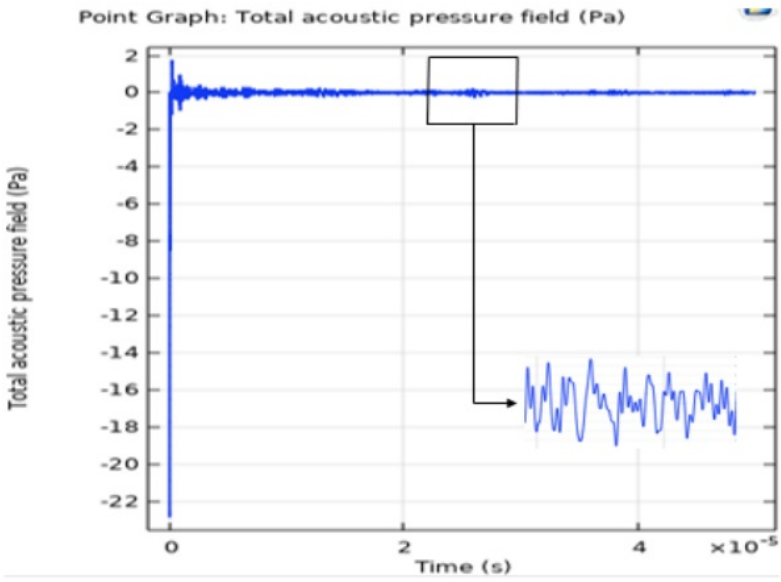

Figure 31:COMSOL results for 10MHz

The following figure illustrates the resulting spectrum of acoustic pressure caused by rupture artery at 10MHz frequency. Figure 32a demonstrates that the signal is coming

towards the artery, and figure 32b demonstrates the signal after hitting the artery. Afterward, figure 32c illustrates that the signal is entering into the blood after passing the ruptured artery, and it is returning to the sensor after hitting the second artery. This process continues until the user-selected time duration is finished. Moreover, figure 32d shows the spectrum of the result.

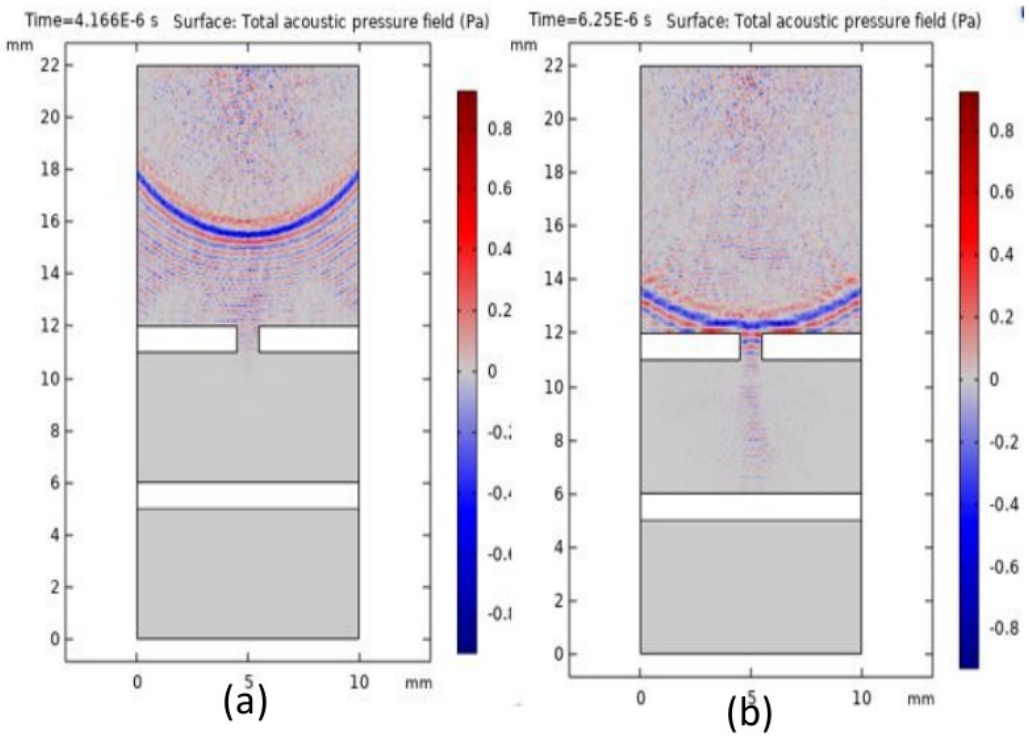

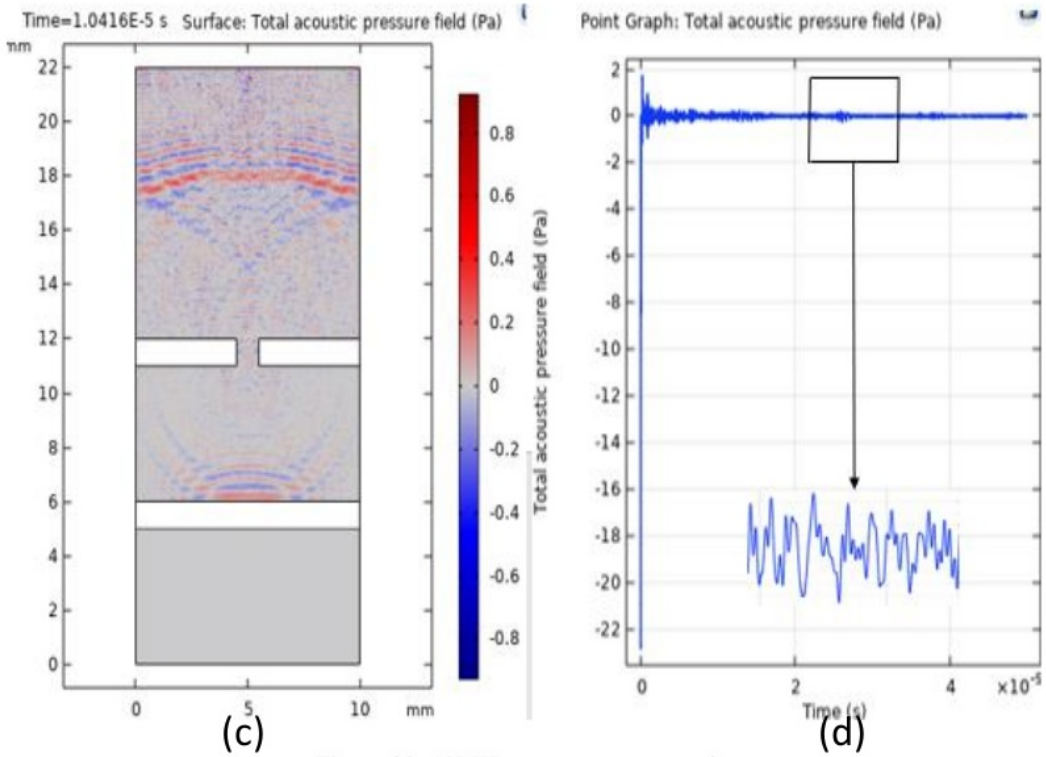

Figure 32: 10MHz rupture artery results

3.11. Simulation results for 1MHz and 10 MHz

The simulation illustrates the COMSOL results for frequency values 1MHz and 10 MHz in the below section. In the proposed model, the time domain and frequency domain is used. Time-domain results show how a signal change over time, and frequency-domain results show how much of the signal lies within each given frequency band over a range of frequencies. All the proposed model values are given in table 14, and all the models are illustrated in figure 33.

Figure 33: Different simulation models with varying rupture sizes

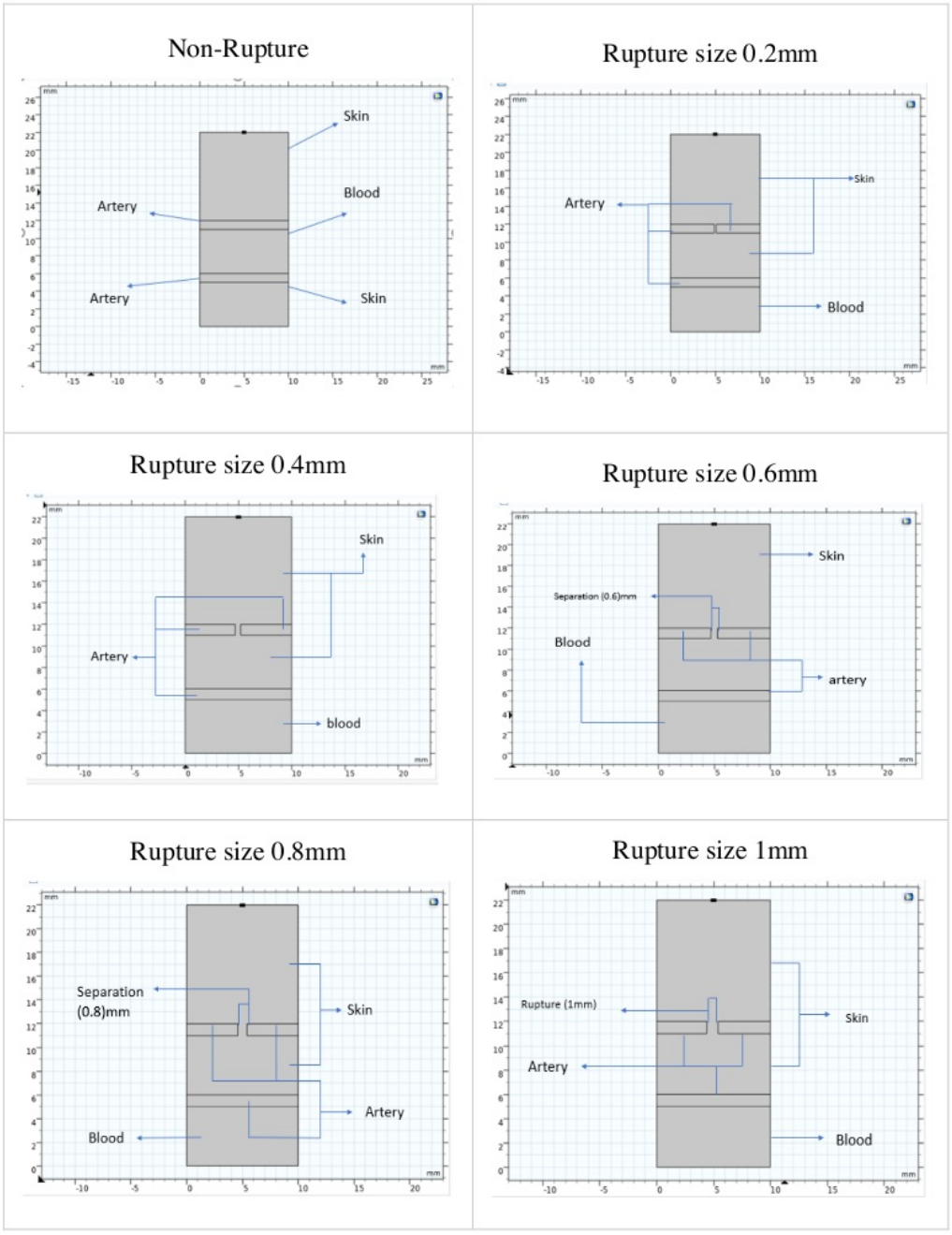

Table 12: All different module value

No	Dimensions	non-Rupture	Rupture (0.2mm)	Rupture (0.4mm)	Rupture (0.6mm)	Rupture (0.8mm)	Rupture (1mm)
skin(r1)	Width	10	10	10	10	10	10
	Height	10	16	16	16	16	16
	X	0	0	0	0	0	0
	Y	12	6	6	6	6	6
Artery(r2)	Width	10	4.9	4.8	4.7	4.6	4.5
	Height	1	1	1	1	1	1
	X	0	0	0	0	0	0
	Y	11	11	11	11	11	11
Blood Part(r4)	Width	10	10	10	10	10	10
	Height	5	5	5	5	5	5
	X	0	0	0	0	0	0
	Y	6	0	0	0	0	0
Artery(r3)	Width	10	4.9	4.8	4.7	4.6	4.5
	Height	1	1	1	1	1	1
	X	0	5.1	5.2	5.3	5.4	5.5
	Y	5	11	11	11	11	11
Artery(r5)	Width	-	10	10	10	10	10
	Height	-	1	1	1	1	1
	X	-	0	0	0	0	0

	Y	-	5	5	5	5	5
Skin2(r5)	Width	10	-	-	-	-	-
	Height	5	-	-	-	-	-
	X	0	-	-	-	-	-
	Y	0	-	-	-	-	-
Point2(pt1)	Width	-	-	-	-	-	-
	Height	-	-	-	-	-	-
	X	4.9	4.9	4.9	4.9	4.9	4.9
	Y	22	22	22	22	22	22
Point2(pt2)	Width	-	-	-	-	-	-
	Height	-	-	-	-	-	-
	X	5.1	5.1	5.1	5.1	5.1	5.1
	Y	22	22	22	22	22	22

3.12. 1MHz

The parameters of the time-domain simulation for the frequency of 1 MHz are shown in table 15. Different simulations with the same value of (1MHz) are done, but different rupture values (1mm, 0.2mm, 0.4mm, 0.6mm, 0.8mm, and non-rupture) are shown in table 14. All the results for the mentioned models are different from each other. Comparing the time-domain results (non-rupture and 0.2mm rupture) and the frequency domain (non-rupture and 0.2mm rupture) are done. Figure 34a shows the time domain results, and figure 34b shows the frequency domain with non-rupture and 0.2mm rupture. The parameters for 1MHz frequency are given in the below table.

Table 13: 1MHz simulation parameter

Name	Expression	Description
Amplitude	10	10
Period	0.5	0.5
Frequency	1000000	$1E^{6}$
simulation time	500/frequency	$5E^{-5}$
Simulation step	1/(100*frequency)	$1E^{-8}$
Skin Speed of sound	1540	1540

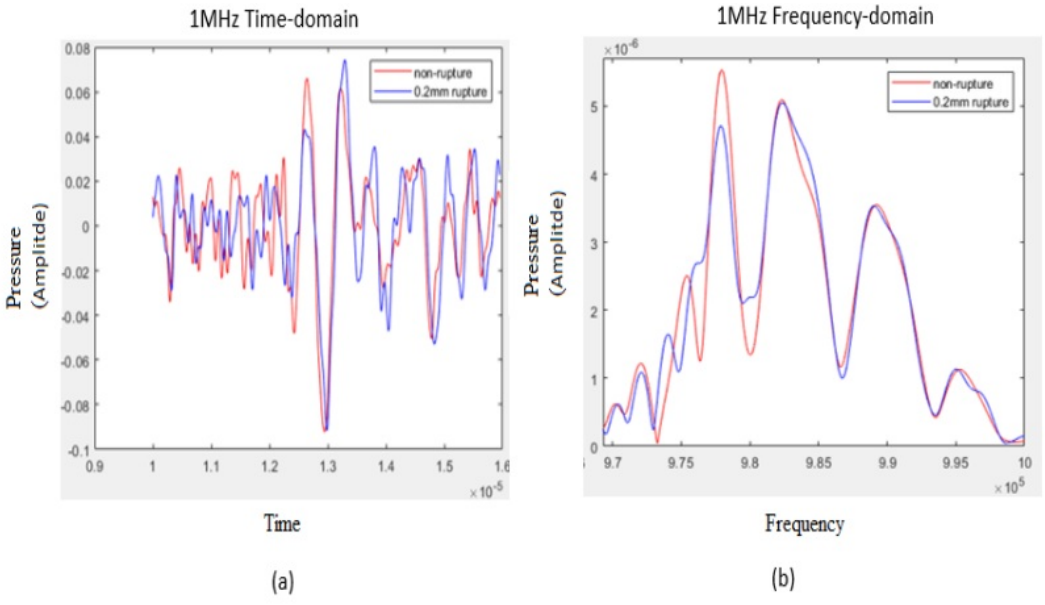

Figure 34: (a) time-domain results and (b) Frequency domain results. This figure has shown the difference between (non-rupture and 0.2mm rupture)

The parameters of the time-domain simulation for the frequency of 1 MHz are shown in table 15. Comparing the time-domain results (non-rupture and 0.4mm rupture) and the frequency domain (non-rupture and 0.4 mm rupture) are done. Figure 35a shows the time domain results, and figure 35b shows the frequency domain with non-rupture and 0.4mm rupture.

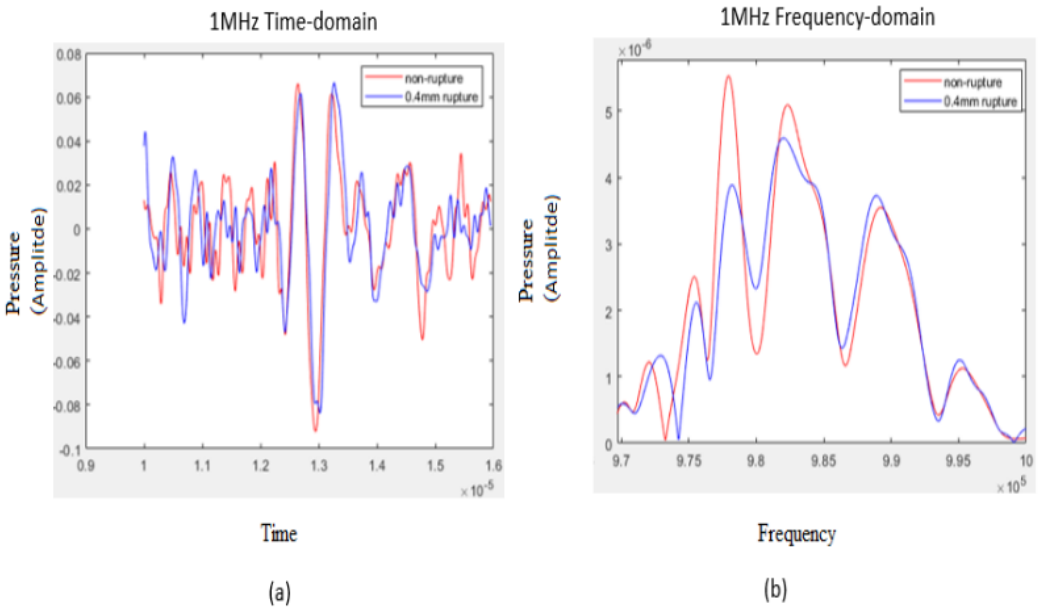

Figure 35: 1MHz (a) time-domain results and (b) frequency-domain results. This figure has shown the difference between (non-rupture and 0.4mm rupture)

The parameters of the time-domain simulation for the frequency of 1 MHz are shown in table 15. Comparing the time-domain results (non-rupture and 1mm Rupture) and the frequency domain (non-rupture and 0.6mm rupture) are done. Figure 36a shows the time domain results, and figure 36b shows the frequency domain with non-rupture and 0.6mm rupture.

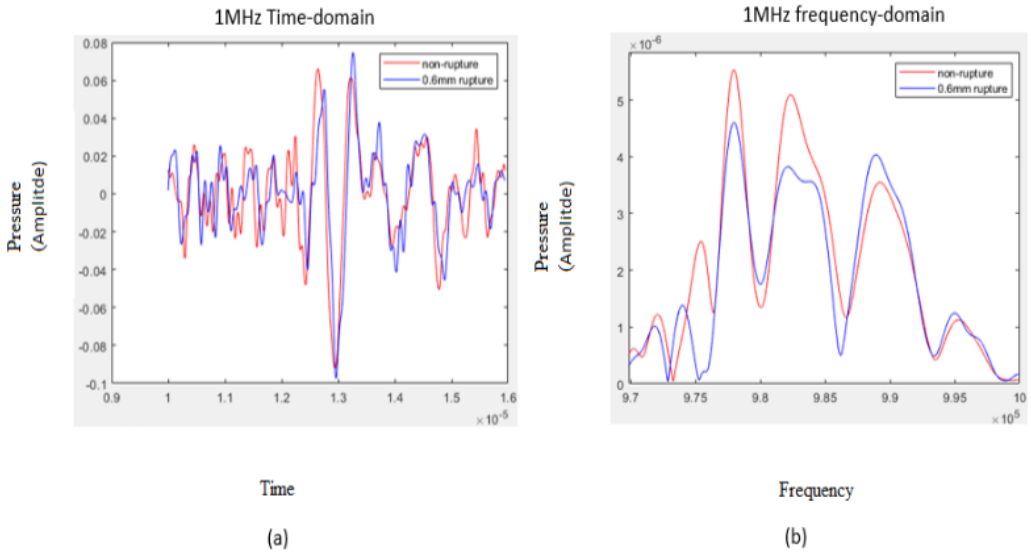

Figure 36:1MHz (a) time domain and (b) Frequency domain results. This figure has shown the difference between (non-rupture and 0.6mm rupture)

The parameters of the time-domain simulation for the frequency of 1 MHz are shown in table 15. Comparing the time-domain results (non-rupture and 0.8mm rupture) and the frequency domain (non-rupture and 0.8mm rupture) are done. Figure 37a shows the time domain results, and figure 37b shows the frequency domain with non-rupture and 0.8mm rupture.

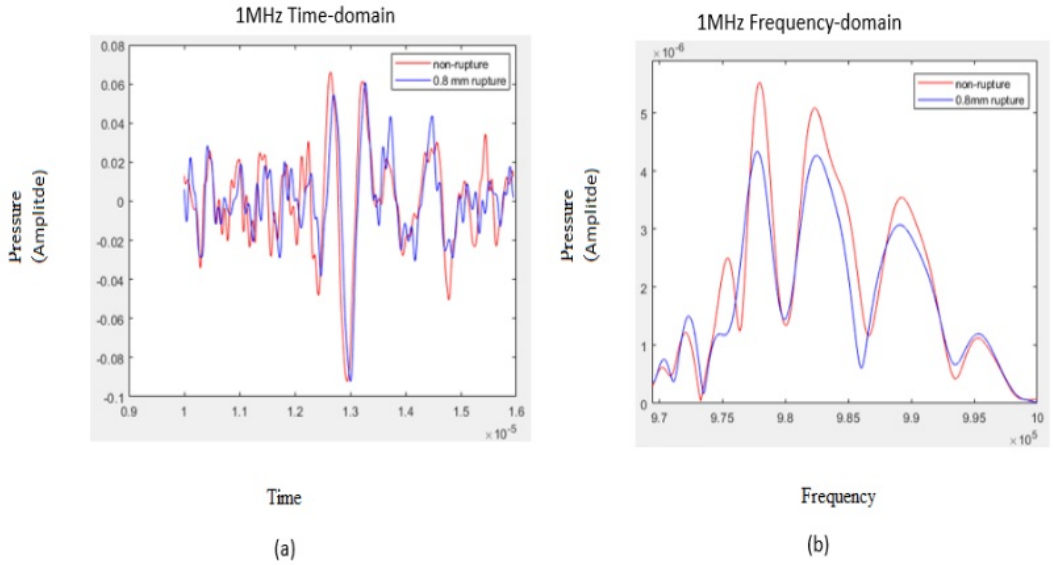

Figure 37:1MHz (a) time domain and (b) Frequency domain results. This figure has shown the difference between (non-rupture and 0.8mm rupture)

The parameters of the time-domain simulation for the frequency of 1 MHz are shown in table 15. Comparing the time-domain results (non-rupture and 1mm Rupture) and the frequency domain (non-rupture and 1mm rupture) are done. Figure 38a shows the time domain results, and figure 38b shows the frequency domain with non-rupture and 1mm rupture.

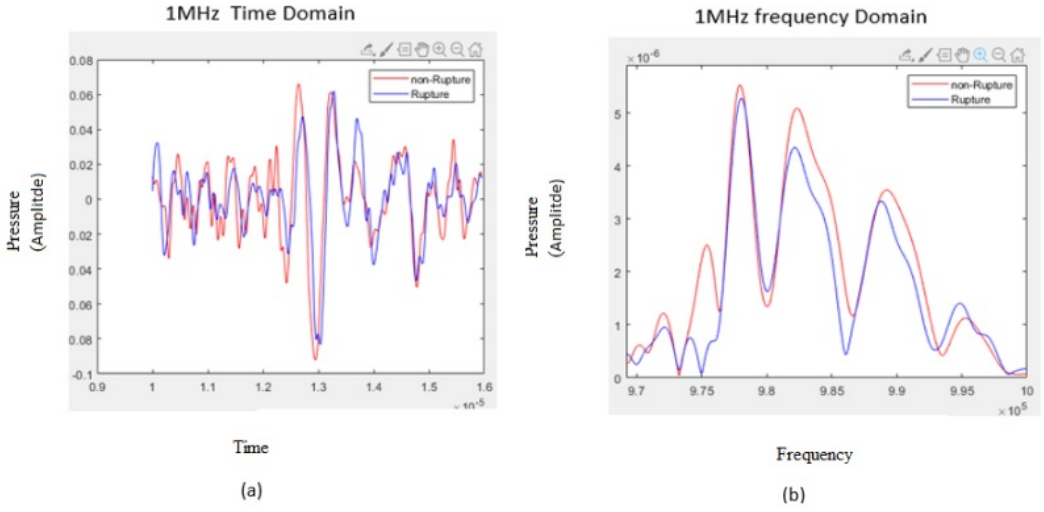

Figure 38: 1MHz (a) time domain and (b) frequency-domain results. This figure has shown the difference between (non-rupture and 1mm rupture)

The below graph illustrates the artery rupture graph for the 1Mhz frequency pressure value. It can be visualized that all the graphs' reflections are different from different rupture values. For instance, the rupture value 0.2mm reflection is different than 0.4mm rupture reflection. Moreover, the model is tested upon different rupture sizes i.e., 0.2mm, 0.4mm, 0.6mm, 0.8mm, 1mm.

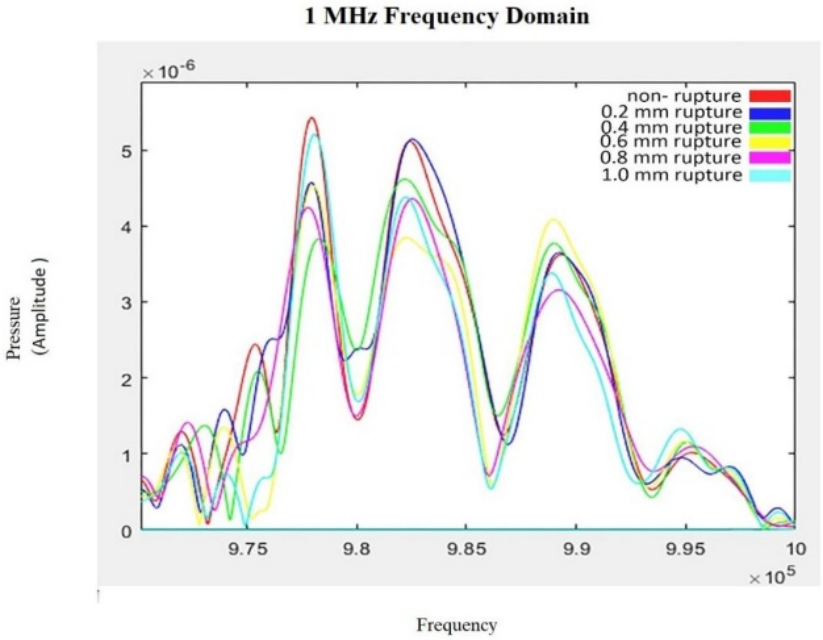

Figure 39: Comparison of artery rupture between 0.2mm-1mm

3.13. 10MHz

The parameters of the time-domain simulation for the frequency of 10 MHz are shown in table 16. Different simulations with the same value of (10MHz) are done, but different rupture values are shown in table 14. All the results for the mentioned models are different from each other. Comparing the time-domain results (non-rupture and 0.2mm rupture) and the frequency domain (non-rupture and 0.2mm rupture) are done. Figure 40a shows the time domain results, and figure 40b shows the frequency domain with non-rupture and 0.2mm rupture. The parameters for 10MHz frequency are given in the below table.

Table 14: 10MHz simulation parameter

Name	Expression	Description
Amplitude	10	10
Period	0.5	0.5
Frequency	10000000	$1E^{7}$
simulation step	1/(100*frequency)	$1E^{-9}$
Simulation time	500/frequency	$5E^{-5}$
Skin Speed of sound	1540	1540

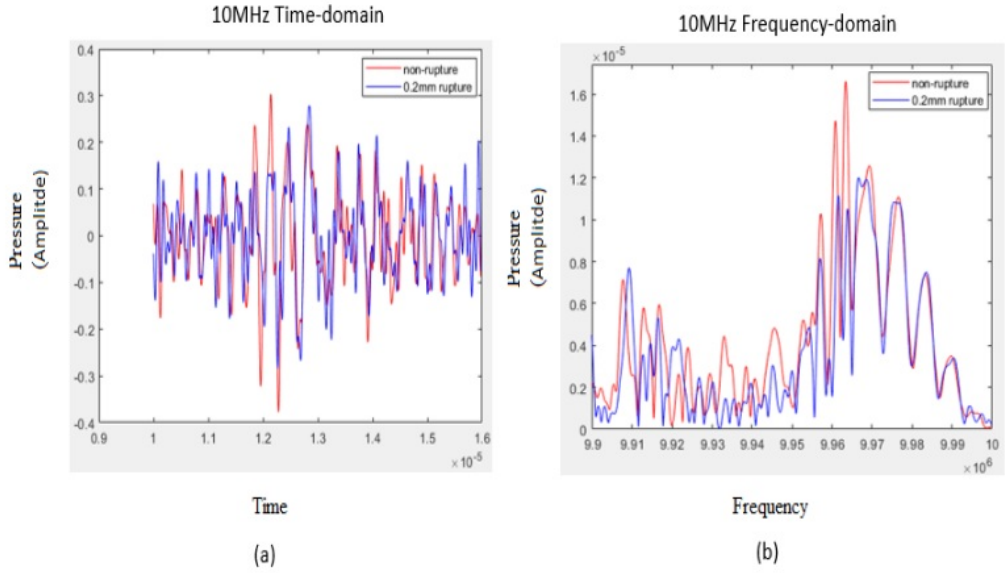

Figure 40: 10MHz (a) time domain and (b) frequency-domain results. This figure has shown the difference between (non-rupture and 0.2mm rupture)

The parameters of the time-domain simulation for the frequency of 10 MHz are shown in table 16. Comparing the time-domain results (non-rupture and 0.4mm rupture) and

the frequency domain (non-rupture and 0.4mm rupture) are done. Figure 41a shows the time domain results and the 41b frequency domain with non-rupture and 0.4mm rupture.

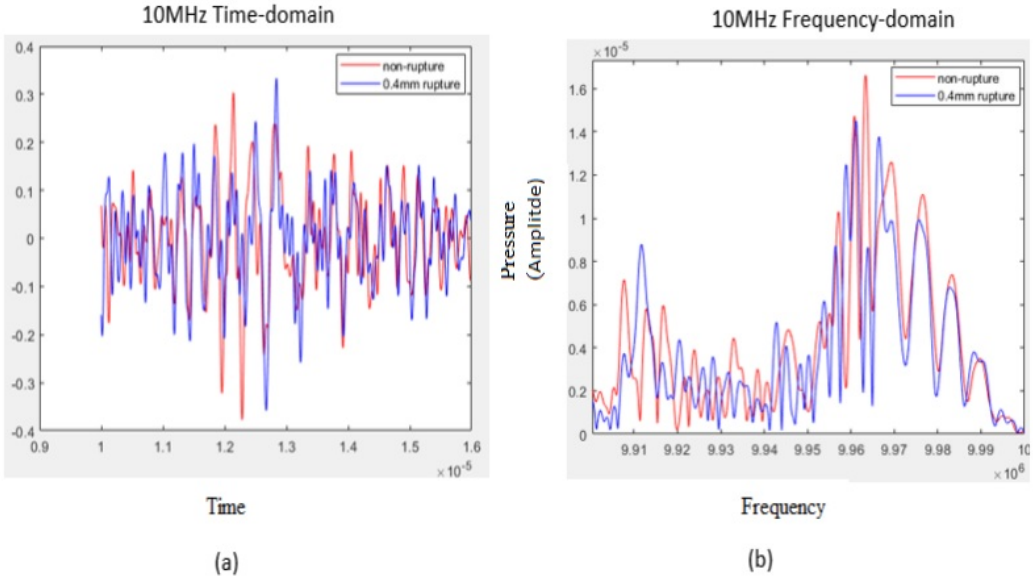

Figure 41: 10MHz (a) time domain and (b) frequency-domain results. This figure has shown the difference between (non-rupture and 0.4 mm rupture)

The parameters of the time-domain simulation for the frequency of 10 MHz are shown in table 16. Comparing the time-domain results (non-rupture and 0.6mm rupture) and the frequency domain (non-rupture and 0.6 mm rupture) are done. Figure 42a shows the time domain results, and figure 42b shows the frequency domain with non-rupture and 0.6mm rupture.

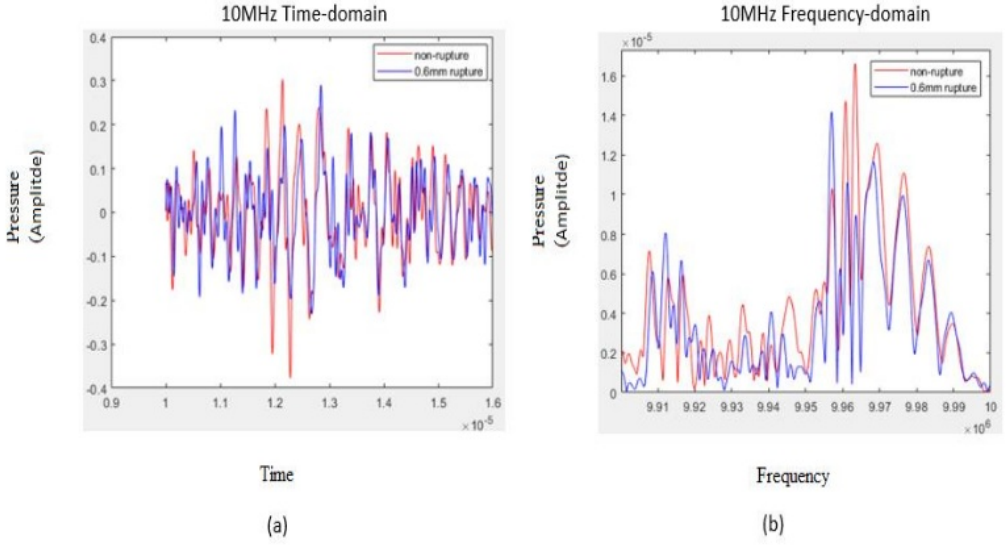

Figure 42: 10MHz (a) time domain and (b) frequency-domain results. This figure has shown the difference between (non-rupture and 0.6 mm rupture)

The parameters of the time-domain simulation for the frequency of 10 MHz are shown in table 16. Comparing the time-domain results (non-rupture and 0.8mm rupture) and the frequency domain (non-rupture and 0.8mm rupture) are done. Figure 43a shows the time domain results, and figure 43b shows the frequency domain with non-rupture and 0.8mm rupture.

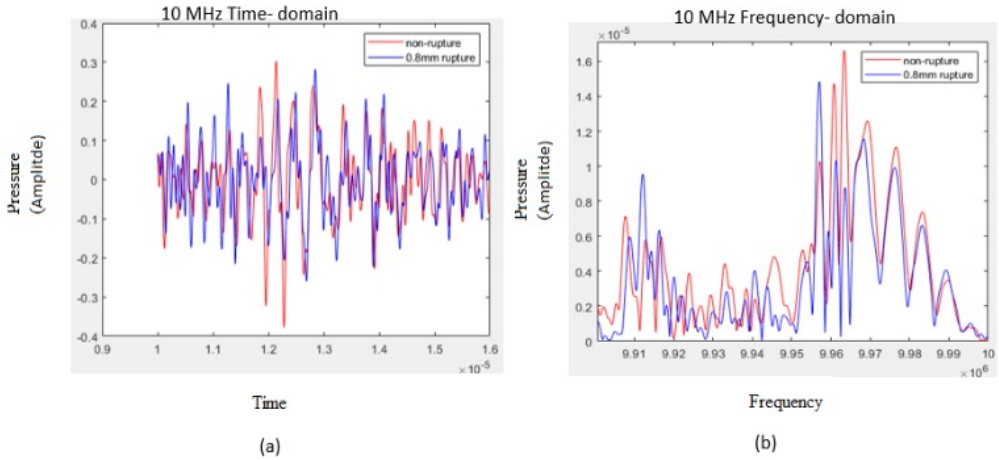

Figure 43: 10MHz (a) time domain and (b) frequency-domain results. This figure has shown the difference between (non-rupture and 0.8 mm rupture)

The parameters of the time-domain simulation for the frequency of 10 MHz are shown in table 16. Comparing the time-domain results (non-rupture and 1mm Rupture) and the frequency domain (non-rupture and 1mm rupture) are done. Figure 44a shows the time domain results, and figure 44b shows the frequency domain with non-rupture and 1mm rupture.

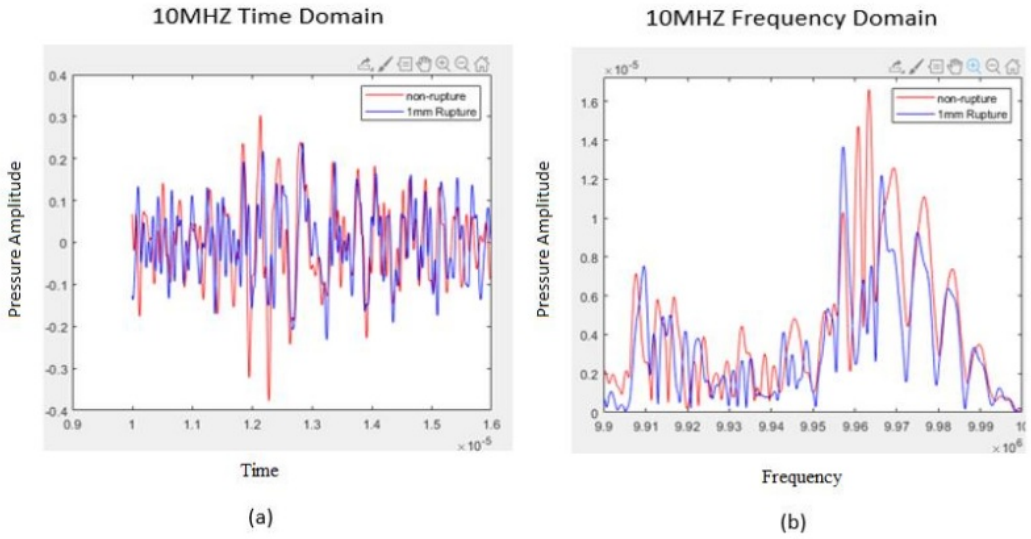

Figure 44: 10MHz (a) time-domain and (b) frequency-domain results. This figure has shown the difference between (non-rupture and 1mm rupture)

The below graph illustrates the frequency pressure graph for the 10Mhz value. It can be visualized that all the graphs' reflections are different from different rupture values. For instance, the rupture value 0.2mm reflection is different than 0.4mm rupture reflection. Moreover, the model is tested upon different rupture sizes i.e., 0.2millimeter, 0.4 millimeter, 0.6 millimeter, 0.8 millimeter, 1 millimeter.

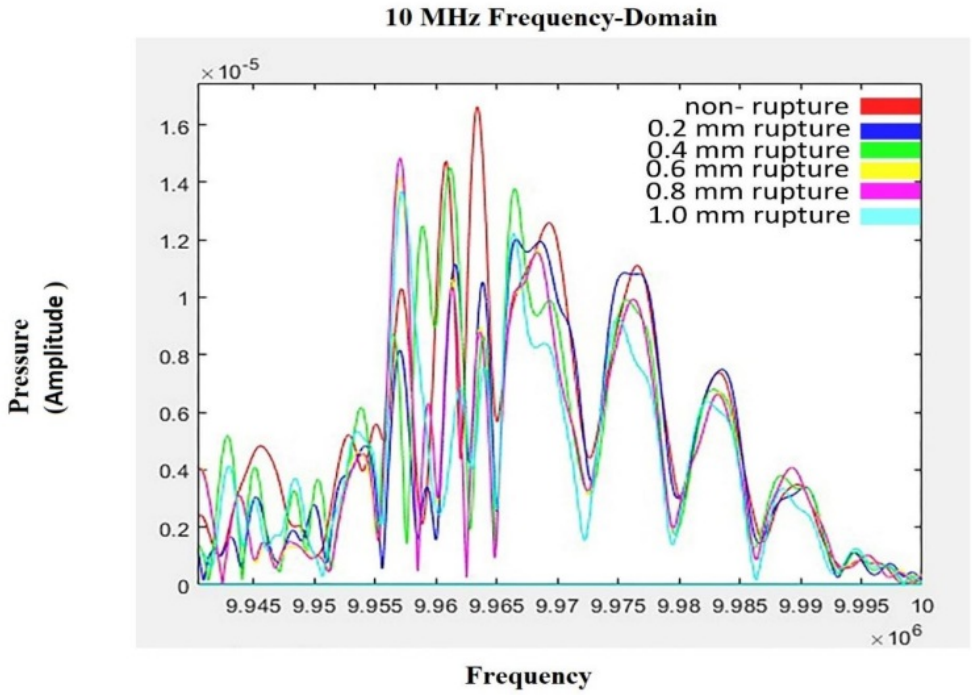

Figure 45: Comparison of artery rupture between 0.2mm-1mm

From the tables mentioned above, we can conclude that there is not much difference between the time domain signals of a non-ruptured and ruptured artery. The FFT's of the ultrasonic echoes of non-ruptured and ruptured signals are not much different from each other at 1Mhz. The reason for that is the wavelength of sound is around (1540/10000000) $1.5E^{-3}$mm, which is smaller than the rupture size. The significant differences in the FFT's at 10 MHz are observed. By designing proper filters, detection of a rupture's presence and the size of a rupture can be determined.

The graph shows that on 10MHz frequency, the rupture size is 0.2-millimeter with 10 different time slots, also show the non- rupture spectrum on 10 different time slots. Further more, the difference between rupture 0.4-millimeter, 0.6-millimeter, 0.8-millimeter, and 1-millimeter is briefly discussed in the next section with the difference between rupture and non-rupture.

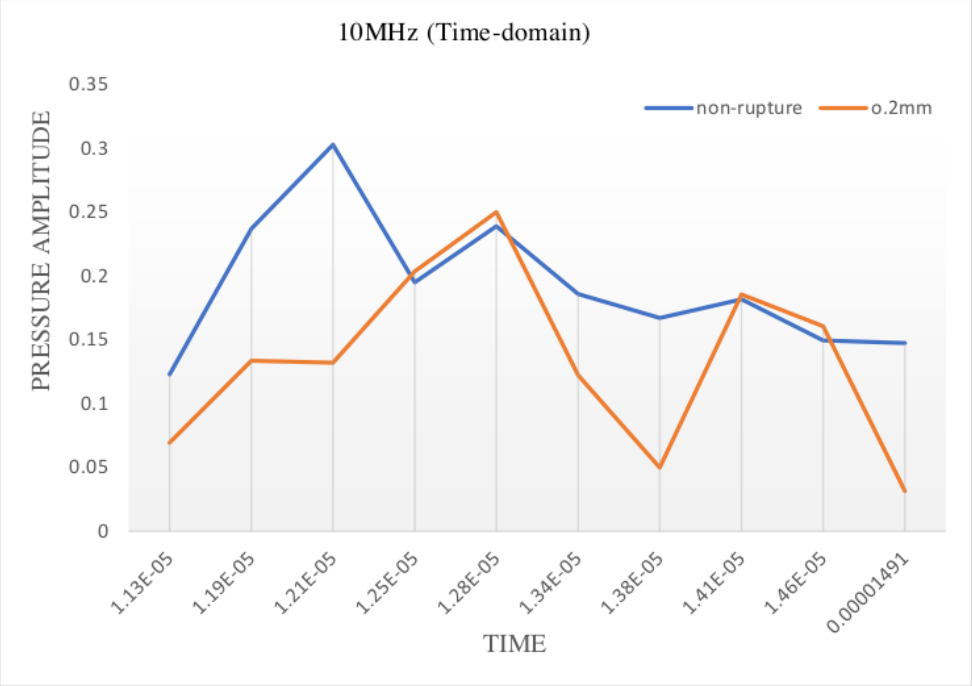

Figure 46: 10MHz (Time domain) graph.

The below graph illustrates the difference between rupture and non-rupture when using 10MHz frequency on the time-domain. The graph shows that when the rupture's size was taken as 0.2-millimeter, 0.4-millimeter, 0.6-millimeter, 0.8-millimeter, and 1-millimeter at 10 different times, what was the rupture and non-rupture at different time. When 10MHz frequency is used on 0.2-millimeter rupture size on $11.29e^{-6}$ (μ_s), the difference between rupture and non-rupture is 0.05349 (Ps). Similarly, when 10MHz frequency is used on the 0.2-millimeter size on $12.14e^{-6}$ (μ_s), there was a 0.1708 (Ps) difference between rupture and non-rupture. Moreover, the same procedure is used on the rupture size 0.4-millimeter, 0.6-millimeter, 0.8- millimeter, and 1–millimeter. The different differences are found at different times between rupture and non-rupture, fully demonstrated in the below graph.

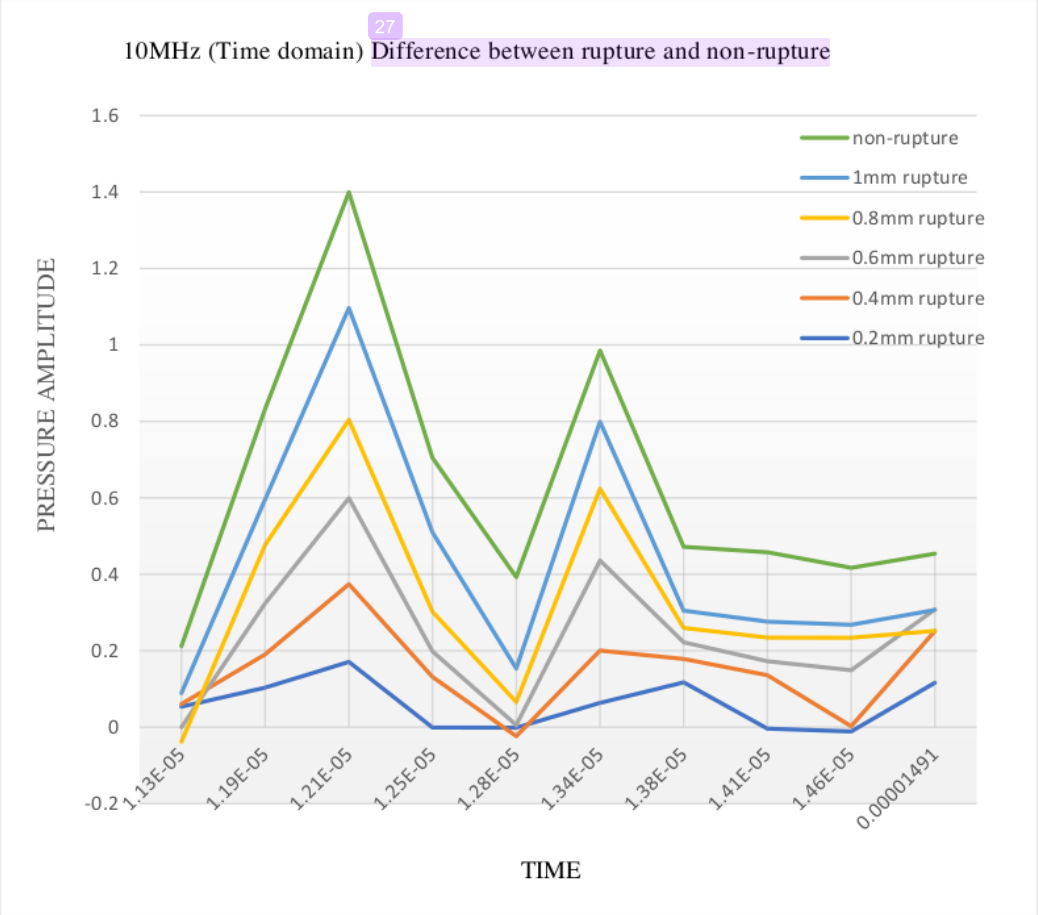

Figure 47: 10MHz (Time domain) difference between rupture & non-rupture graph.

The graph below illustrates the difference between rupture and non-rupture when using 10MHz frequency on the frequency-domain. The graph shows that when the rupture's size was taken as 0.2-millimeter, 0.4-millimeter, 0.6-millimeter, 0.8-millimeter, and 1-millimeter at 10 different times, what was the rupture and non-rupture at different time. When 10MHz frequency is used on 0.2-millimeter rupture size on 990800 (Hz), the difference between rupture and non-rupture is $7.087e^{-5}$ [m] (The SI unit of amplitude is the meter [m]). Similarly, when 10MHz frequency is used on the 0.2-millimeter size on 996300 (Hz), there was a $1.661e^{-5}$ [m] difference between rupture and non-rupture. Moreover, the same procedure is used on the rupture size 0.4-millimeter, 0.6- millimeter, 0.8- millimeter, and 1–

millimeter. The different differences are found at the different times between rupture and non-rupture, which is fully demonstrated in the below graph.

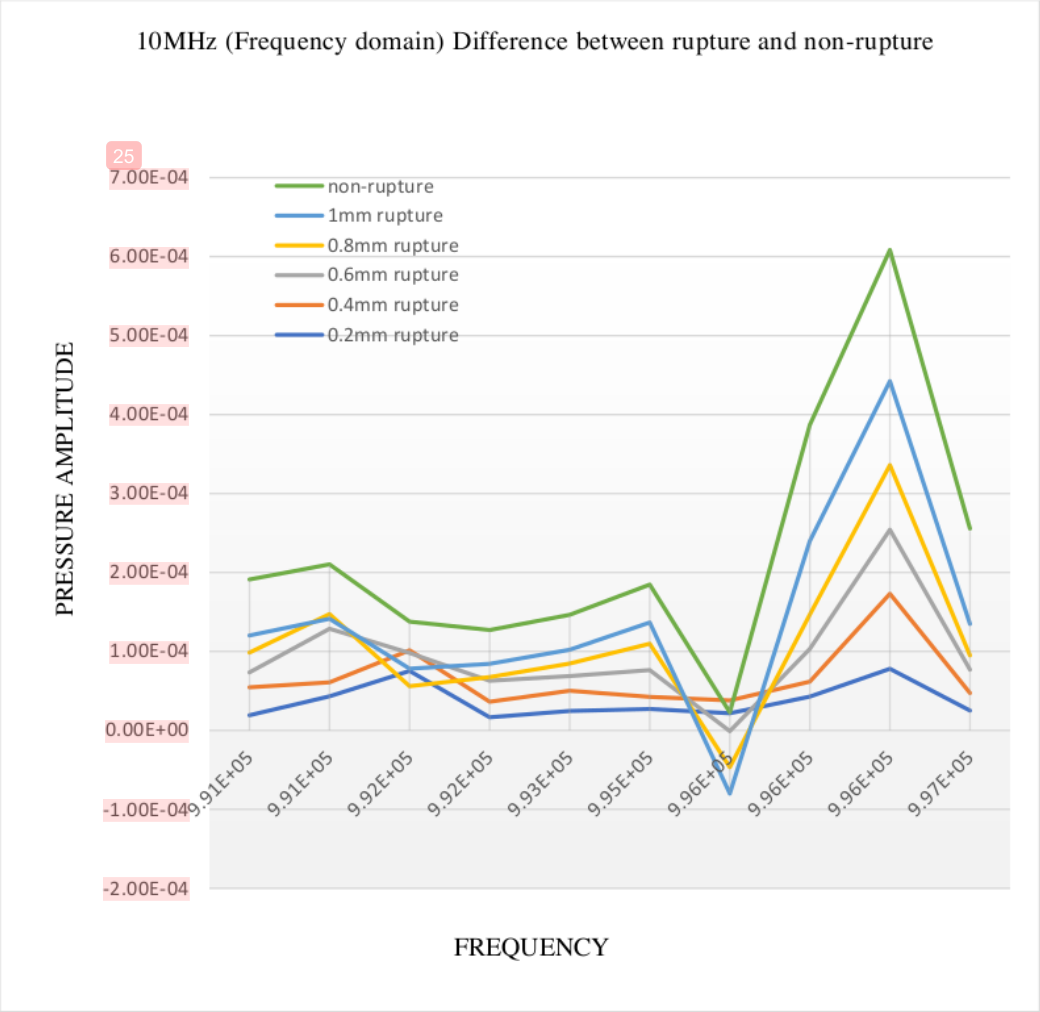

Figure 48: 10MHz (Frequency domain) difference between rupture & non-rupture graph.

DESIGN AND FABRICATION

4.1. Design

The below figure illustrates the five different layers, and the sensor is placed on the skin. After providing input, the ultrasonic waves cross the skin and collides with an artery. If the artery is non-ruptured, the signal will be reversed from the first artery towards the sensor, and it will show the spectrum result. If the artery is ruptured, the echo signature will be different from the input signal.

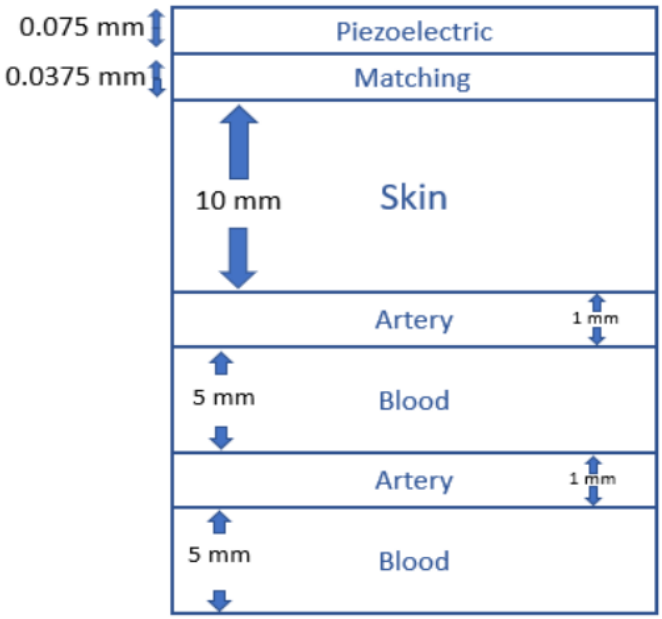

Figure 49: The proposed sensor design

The most important component of such device is the piezoelectric element. A number of factors involved in choosing a proper piezoelectric material for receiving and transmitting the ultrasonic wave. They include piezoelectric properties, stability, and the strength of the material. The surfaces of the element are electrodes with fired-on silver or sputtered chrome–gold. The housing is metallic or plastic. An acoustic isolating material is placed between piezoelectric element & housing to prevent ringing of the housing, that follows the piezoelectric element's vibration. By considering the two surfaces of the piezoelectric

element as two independent vibrators, one can easily see that the resonant frequencies for such a transducer, $c_{p,}$ is the acoustic wave velocity in the transducer material, L is the thickness of the piezoelectric material, n is an odd integer.

$$f_0 = nc_{p/2L} \qquad (7)$$

By considering the two surfaces of the piezoelectric element as two independent vibrators, one can easily see that the resonant frequencies for such a transducer, c_p is the acoustic wave velocity in the transducer material, L is equal to odd multiples of one-half wavelength, where λ_p is the wavelength in the piezoelectric material.

$$L = n\,{}^{\lambda_p}/_{2} \qquad (8)$$

This section explains some equations used for device design to find the model's diameter, piezoelectric thickness, and matching layer thickness; the frequency is selected to be 10 MHz due to the simulation results explained above. The sound of speed is 1540 m/s, and the depth is 10 mm since the arteries are at this depth. The region where axial pressure oscillates is called the near-field. N is the near field of length (depth) where shown in equation (3). The wavelength λ is calculated using the formula $\lambda = \frac{c}{f} = 0.15\ mm$, for given values of c and f. D is the diameter of the piezoelectric transducer that is:

$$D^2 = 4\text{NL}\,\lambda. \qquad (9)$$

Therefore, the diameter becomes 2.45 mm. A piezoelectrical thickness is equal to half of the wavelength that is ${}^{\lambda}/_{2} = 0.075mm$, and the matching layer thickness is quarter of the wavelength that is $\frac{\lambda}{4} = 0.0375\text{mm}$.

4.2. Fabrication

The device fabrication consists of successive deposition and patterning of metal and piezoelectric materials on a flexible substrate. A variety of different strategies can be applied in this respect. The substrate can be chosen as a thin layer of plastic material, acrylic, or PDMS, shown in figure 39. A 20 nm-thick Cr and 100 nm-thick Au layers are deposited using sputtering initially. Next, a thin layer of piezoelectric material such as PZT or PVDF should be deposited. In this respect, PZT sputtering can be applied. Finally, the top layer metal is formed using sputtering the same thickness Cr/Au as described above. Since the

tolerances are on the order of millimeters, shadow masking can be used for a straight-forward patterning.

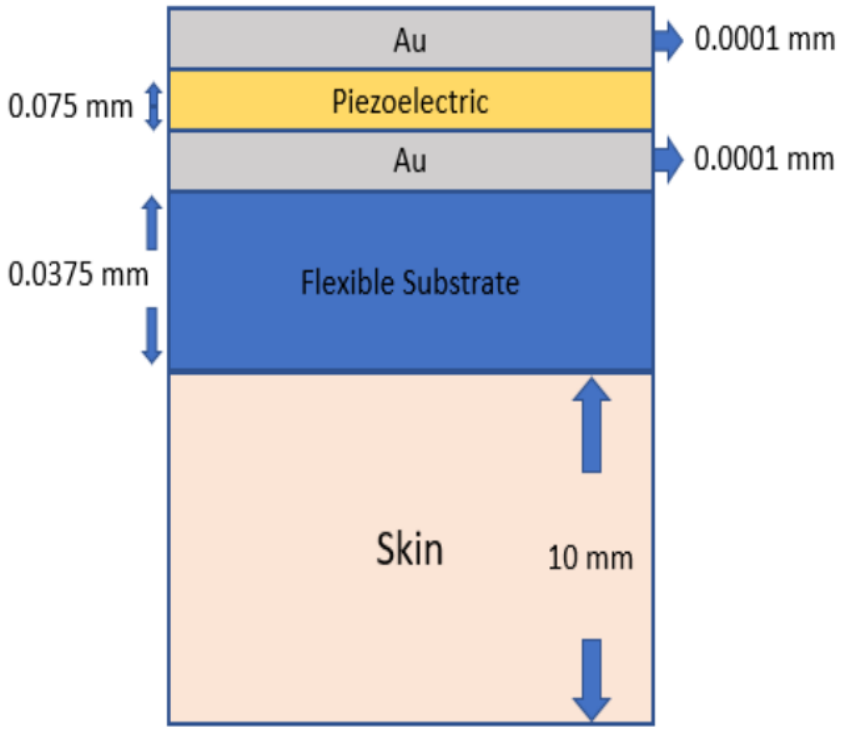

Figure 50: Fabrication

CONCLUSION AND FUTURE WORK

5.1. Conclusion

This work is analyzing and developing an ultrasonic biosensor theoretically to detect arterial rupture. Ultrasonics is used in different prognostics, but in this work, ultrasonics is used for the first time for detecting aneurysm disease (artery rupture) by utilizing an on-skin transducer. This disease occurs when a part of an artery wall weakens, resulting in the artery's abnormal enlargement. To detect this condition of the artery, doctors apply different tests such as (ACG, CT scan, CRB blood test, etc.). When an aneurysm is detected in a patient, the best approach to counter this disease is by adding a stent to the artery. The stent addition may be relatively straight forward for young patients, but it is risky for older people. Therefore, the best solution is to wait for surgery in some cases until the artery starts rupturing. The waiting period depends on the patient's condition. If the artery starts rupturing, the stent should be applied to avoid the risks.

This sensor detects this last possible moment when the artery starts rupturing. This sensor will delay the risks to artery stents insertion and gives the maximum time to prevent surgery. The sensor is used to detect the artery rupturing in the early stages. In this research, the proposed design of an ultrasonic piezoelectric sensor detects the artery rupture. A sensor is placed on the skin aligned with the aneurysm location. The signals received and processed by the sensor will be different for each rupture size, which provides the idea about rupture size. This sensor was developed on COMSOL. In the proposed model, the time domain and frequency domain analyses are used. Time-domain results show how a signal change over time, and frequency-domain results show how much of the signal lies within each given frequency band over a range of frequencies.

The different simulated models (non-ruptured, 0.2mm artery rupture, 0.4mm artery rupture, 0.6mm artery rupture, 0.8mm artery rupture, 1mm artery rupture) were performed. Initially, a frequency of 1 MHz is used to detect the artery rupture. But at this frequency, sensors do not show a significant difference between the frequency spectrums of the non-ruptured and rupture artery's ultrasonic echoes. However, significant differences were

observed between the frequency spectrums of the normal and ruptured artery's ultrasonic echoes by using a frequency of 10 MHz Comparison between the results of ruptured and non-ruptured arteries by using the frequency domain is done. After providing input, the signal crosses the skin and collides with an artery. If an artery has a rupture, the signal crosses the artery and inter into the blood. Afterward, it hits the second artery and reverses back to the skin with outcomes, and the sensor shows the resulting spectrum. Based on this study, a device design and fabrication process flow were developed.

5.2. Future work

This work demonstrated theoretically that an on-skin ultrasonic transducer could detect the arterial rupture by using the frequency domain analysis. A transducer design, along with a fabrication process flow, was developed. The future work will focus on applying the fabrication to realize the first transducers, as well as on the detailed testing and characterization of the device. The results will pave the way for the development of a vital product for patients with aneurysm diseases.

REFERENCES

1. Ou, S.H.; Wu, M.C.; Chou, T.C.; Liu, C.C, 2004, "Polyacrylamide gels with electrostatic functional groups for the imprinting of lysozyme," Anal. Chim. Acta, 2004, 504, 163–166.
2. Ivnitski, D.; Abdel-Hamid, I.; Atanasov, P.; Wilkins, E. 1999, "Biosensor for detection of pathogenic bacteria. Biosens", Bioelectron., 14, 599–624.
3. Berna, A, 2010, "Metal oxide sensors for electronic noses and their application to food analysis," Sensors 2010, 10, 3882–3910.
4. Clinical Laboratory, Immunoassay Systems, September 10, 2020 02:35 PM, "Immunoassay Analyzer Model PATHFAST," www.trademed.com/products/7826/Immunoassay-Analyzer.html
5. Accurate temperature control and sensing, September 2020 03:15 PM , "infrared thermometer," https://www.atcsensing.com/how-accurate-is-a-medical-grade-infrared-thermometer/.
6. Proteus, September 23 ,2020 11:20 AM, Multi parameter water quality sensor, "quality sensor," https://www.proteus instruments.com/proteus-bod-multiparameter-water-quality-meter/.
7. Zahan success formula, Oct 10,2020, 10: 35 AM, " Dental Colorimeter(ZFX Shade)," medicalexpo.com/prod/zfx/product-74624-461040.html.
8. One touch ultra2, Oct 10,2020, 02: 35 PM "Blood glucose monitoring," https://www.onetouch.com/products/glucose-meters/onetouch-ultra2
9. Dentalcompare, Oct 15,2020, 01: 00 PM “visOra DR Digital Sensor System from CIEOS, Inc.,” https://www.dentalcompare.com/4448-Dental-Digital-Radiography-Digital-Dental-X-Ray-Intraoral/38997-VISORAdr/
10. Citizen science grid, Oct 10,2020, 04: 50 PM "Blood pressure monitors: Managing health," https://csgrid.org/csg/team_display.php?teamid=424759.
11. Probo medical, DATE.10- 11- 2020, TIME. 14:20." Philips IU22 Ultrasound Transducer Guide", https://www.probomedical.com/philips-iu22-ultrasound-transducer-guide/.

12. Become a sonographer, DATE.10- 11- 2020, TIME. 14:25 "B - modeultrasoundinnovations," https://becomeasonographer.weebly.com/b-mode-ultrasound-innovations.html.
13. Turandot Saul, MD, RDMS, RDCS, Sebastian D. Siadecki, MD, Rachel Berkowitz, MD, Gabriel Rose, DO, Danielle Matilsky, MD, and Allison Sauler, MD, 2015, "M-mode ultrasound applications for the emergency medicine," The Journal of Emergency Medicine, Vol. 49, No. 5, pp. 686–692.
14. Vikas Diagnostics, DATE.12-11-2020, TIME. 10:20," 4D color ultrasound, ", https://www.vikasdiagnostics.com/3d-4d-ultrasound/.
15. Daniel Hänggi , 2017 , "Medically reviewed by Seunggu Han, M.D., Written by Markus MacGill on November 28, 2017.
16. Medingoo.com, November 5,2020, "Fusiform aneurysm," https://www.medigoo.com/articles/fusiform- aneurysm/
17. Pinclipart, DATE.12- 11- 2020, TIME. 12:00, "Intracranial Berry Aneurysm Clipart," https://www.pinclipart.com/pindetail/iJxhiT_download-the-image-intracranial-berry-aneurysm-clipart/.
18. N sakalihasan, R limit, O.D Defawe, 2005, "Abdominal aortic aneurysm," Vol 365 April 30, 2005.
19. Medical plus, November 17,2020 04:00 PM , "Abdominal aortic aneurysm," https://medlineplus.gov/ency/article/000162.htm
20. Interson, DATE.12-11-2020, TIME. 14:20, "The Role Of Office-Based Ultrasound in Screening for Abdominal Aortic Aneurysms," https://interson.com/tech-talk/the-role-of-office-based-ultrasound-in-screening-for-abdominal-aortic-aneurysms/.
21. Christopher L. Taylor M.D. 1, Zhong Yuan M.D. 1, Warren R. Selman M.D. 1, Robert A. Ratcheson M.D. 1 and Alfred A. Rimm PhD, 1995, "Cerebral arterial aneurysm formation and rupture in 20,767 elderly patients", hypertension and other risk factors. Volume 83: Issue 5 (Nov 1995).
22. Nam K. Yoon, Scott McNally, Philipp Taussky & Min S. Park, 2016, "Imaging of cerebral aneurysms: a clinical perspective," Neurovascular Imaging volume 2, Article number: 6 (2016).

23. American Stroke Association, DATE.15- 11- 2020, TIME. 16:20, "Cerebral Aneurysms ," https://www.stroke.org/en/about-stroke/types-of-stroke/hemorrhagic-strokes-bleeds/what-you-should-know-about-cerebral-aneurysms.
24. Gyula Gács M.D. 1, Fernando Viñuela M.D. 1, Allan J. Fox M.D. 1 and Charles G. Drake M.D. 1, 1983, "Peripheral aneurysms of the cerebellar arteries," Volume 58: Issue 1 (Jan 1983)
25. Gujarat hospital gastro & vascular Centre, DATE.16- 11- 2020, TIME ,14:20, "Poplitea l Aneurysm," https://www.gujarathospital.in/vascular-surgery/popliteal-aneurysm.html.
26. Ultrasound cases.info, DATE.16-11-2020, TIME. 20:00, "Aneurysm in the right common iliac artery with a hemorrhage in the atheromatous plaque," https://www.ultrasoundcases.info/true-aneurysms-3649/.
27. E. Stanley Crawford, M.D., Salwa A. Saleh, M.D. (by invitation), and John S. Schuessler, M.D. (by invitation), Houston, Texas, 1979, "Treatment of aneurysm," Volume 78 Number 3 September 1979.
28. Bernd Turowski, Stephan Macht, Zolt Kulcsár, Daniel Hänggi, Walter Stummer, 2009 , "Early fatal hemorrhage after endovascular cerebral aneurysm treatment with a flow diverter (SILK-Stent)," 11 December 2009 /Accepted: 26 February 2010 / Published online: 26 March 2010.
29. Matthew A. Cooper* and Victoria T. Singleton, 2007, "A survey of the 2001 to 2005 quartz crystal microbalance biosensor literature", applications of acoustic physics to the analysis of biomolecular interactions 2007 john Wiley & sons, ltd.
30. Liang Sua,∗,Wenzhao Jiaa, Changjun Houb, Yu Leia,∗, 2010, "Microbial biosensors", Elsevier B.V 2010.
31. Aldo Rodaa,b,∗, Luca Ceveninia, Elisa Michelinia,b, Bruce R. Branchinic, 2011, "A portable bioluminescence engineered cell-based biosensor for on-site applications," biosensors and bioelectronics 26 (2011) 3647-3653.
32. Hatice Ceylan Koydemira,c,∗, Haluk Kulaha,b, Canan Ozgenc, Alpaslan Alpd, Guls¸ en Hasc¸ elik d, 2011 "MEMS biosensors for detection of methicillin-resistant Staphylococcus aureus," 2011 Elsevier B.V.s

33. Veeradasan Perumal*,2013, "Uda Hashim, Advances in biosensors: Principle", architec ture and applications§ 2 December 2013
34. Dae Yong Park, Daniel J. Joe, Dong Hyun Kim, Hyewon Park, Jae Hyun Han, Chang Kyu Jeong, Hyelim Park, Jung Gyu Park, Boyoung Joung, and Keon Jae Lee*,2017, "Self-Powered Real-Time Arterial Pulse Monitoring Using, Ultrathin Epidermal Piezoelectric Sensors," DOI: 10.1002/adma.201702308.
35. Xudong Fan∗, Ian M. White, Siyka I. Shopova, Hongying Zhu, Jonathan D. Suter, Yuze Sun, 2008, "optical biosensors," Elsevier B.V. 2008.
36. Anupama Lakshmanan, Zhiyang Jin, Suchita P. Nety, Daniel P. Sawyer, Audrey Lee-Gosselin, Dina Malounda, Mararet B. Swift, David Maresca & Mikhail G. Shapiro, 2020, "Acoustic biosensors for ultrasound imaging of enzyme activity," Nature Chemic al Biology volume 16, pages988–996(2020).
37. Larisa A. Kuznetsova, W. Terence Coakley, "Applications of ultrasound streaming and radiation force in biosensors," 006 Elsevier B.V. All rights reserved.
38. Kerstin Länge & Bastian E. Rapp & Michael Rapp, 2008, "Surface acoustic wave biosensors: a review, Anal Bioanal Chem," (2008) 391:1509–1519
39. Ronen Fogel1, Janice Limson1 and Ashwin A, 2016, "Seshia2 Acoustic biosensors", Essays in Biochemistry (2016) 60 101–110, DOI: 10.1042/EBC20150011
40. A. C. R. Grayson, 2003, "MEMS Devices." April 10, 2003.
41. Ioana Voiculescua, Anis Nurashikin Nordinb, 2011, "Acoustic wave based MEMS devices for biosensing applications," 2011 Elsevier B.V.
42. https://sciencing.com/resonant-frequencies-7569469.html time, 1/18/2021, 5:26 pm.
43. Wanjia Gao, Wenyi Liu,* Yanjun Hu, and Jun Wang, "study of Ultrasonic Near-Field Region in Ultrasonic Liquid-Level Monitoring System," Micromachines (Basel). 2020 Aug; 11(8): 763. Published online 2020 Aug 10.
44. Wanjia Gao, Wenyi Liu, Yanjun Hu, Jun Wang 2020, "Study of Ultrasonic Near-Field Region in Ultrasonic Liquid- Level Monitoring System,"www.mdpi.com/journal/micro machines," Published: 10 August 2020.
45. Ediger E. Franco, Marco A. B. Andrade, Julia C. Adamowski, Flávio Buiochi 2011, "Acoustic Beam Modeling of Ultrasonic Transducers and Arrays Using the Impulse Response and the Discrete Representation Methods," "Paper received 20 May 2009.

Paper accepted 10 August 2011, Technical Editor: Domingos Rade", Vol. XXXIII, No. 4, October-December 2011.

46. Anthony Gachagan, Gordon Hayward, Robert Banks 2005, "A Flexible Piezoelectric Transducer Design for Efficient Generation and Reception of Ultrasonic Lamb Waves," "IEEE transactions on ultrasonics, ferroelectrics, and frequency control," vol. 52, no. 7, July 2005
47. Jan Kredba and Miroslav Holada 2017, "Precision Ultrasonic Range Sensor Using One Piezoelectric Transducer with Impedance Matching and Digital Signal Processing," "(SGS 2017) at the Technical University of Liberec", 2017.

MUHAMMAD HARIS LATIF

INFORME DE ORIGINALIDAD

18%	12%	10%	6%
INDICE DE SIMILITUD	FUENTES DE INTERNET	PUBLICACIONES	TRABAJOS DEL ESTUDIANTE

FUENTES PRIMARIAS

1	doc.comsol.com Fuente de Internet	1%
2	www.mdpi.com Fuente de Internet	1%
3	mafiadoc.com Fuente de Internet	1%
4	Submitted to Cardinal Newman College Trabajo del estudiante	1%
5	myasro.blogspot.com Fuente de Internet	1%
6	www.science.gov Fuente de Internet	1%
7	A. Gachagan. "A flexible piezoelectric transducer design for efficient generation and reception of ultrasonic Lamb waves", IEEE Transactions on Ultrasonics Ferroelectrics and Frequency Control, 7/2005 Publicación	1%

8	X ZHANG. "Medical Imaging", Biomedical Information Technology, 2008 Publicación	1%
9	worldwidescience.org Fuente de Internet	1%
10	www.medicalnewstoday.com Fuente de Internet	<1%
11	search.scielo.org Fuente de Internet	<1%
12	pubs.acs.org Fuente de Internet	<1%
13	sciencing.com Fuente de Internet	<1%
14	Hatice Ceylan Koydemir, Haluk Külah, Canan Özgen, Alpaslan Alp, Gülşen Hasçelik. "MEMS biosensors for detection of methicillin resistant Staphylococcus aureus", Biosensors and Bioelectronics, 2011 Publicación	<1%
15	Jan Kredba, Miroslav Holada. "Precision ultrasonic range sensor using one piezoelectric transducer with impedance matching and digital signal processing", 2017 IEEE International Workshop of Electronics, Control, Measurement, Signals and their Application to Mechatronics	<1%

(ECMSM), 2017
Publicación

16	Submitted to American College of the Middle East Trabajo del estudiante	<1%
17	www.corrosionpedia.com Fuente de Internet	<1%
18	Submitted to Republic Polytechnic Trabajo del estudiante	<1%
19	K. Kirk Shung, Michael B. Smith, Benjamin M.W. Tsui. "Ultrasound", Elsevier BV, 1992 Publicación	<1%
20	docplayer.net Fuente de Internet	<1%
21	Mohamed Abbas, Adel Taha. "Influence of Process Parameters on the Surface Roughness during turning operation of High Strength Steel", Journal of Materials Science Research, 2016. Publicación	<1%
22	Submitted to Ain Shams University Trabajo del estudiante	<1%
23	www.thoughtco.com Fuente de Internet	<1%
24	Cong Peng, Shiqiang Zheng, Ziyuan Huang, Xinxiu Zhou. "Complete Synchronous Vibration	<1%

Suppression for a Variable-Speed Magnetically Suspended Flywheel Using Phase Lead Compensation", IEEE Transactions on Industrial Electronics, 2018
Publicación

25	Submitted to Cranfield University Trabajo del estudiante	<1%
26	Submitted to Shanghai United International School Trabajo del estudiante	<1%
27	Jin Pyeong JEON, Eun Pyo HONG, Jeong Eun KIM, Eun Jin HA, Won-Sang CHO, Young-Je SON, Jae Seung BANG, Chang Wan OH. "Genetic Risk Assessment of Elastin Gene Polymorphisms with Intracranial Aneurysm in Koreans", Neurologia medico-chirurgica, 2018 Publicación	<1%
28	Manal M. Abdus Salam. "Theoretical study of CaO, CaS and CaSe via first-principles calculations", Results in Physics, 2018 Publicación	<1%
29	www.multiphysics.us Fuente de Internet	<1%
30	polen.itu.edu.tr Fuente de Internet	<1%
31	Dae Yong Park, Daniel J. Joe, Dong Hyun Kim,	

	Hyewon Park et al. "Self-Powered Real-Time Arterial Pulse Monitoring Using Ultrathin Epidermal Piezoelectric Sensors", Advanced Materials, 2017 Publicación	<1%
32	Submitted to Ghana Technology University College Trabajo del estudiante	<1%
33	Submitted to Caledonian College of Engineering Trabajo del estudiante	<1%
34	Submitted to Sulaiman AlRajhi Colleges Trabajo del estudiante	<1%
35	Submitted to Universiti Malaysia Perlis Trabajo del estudiante	<1%
36	Wanjia Gao, Wenyi Liu, Yanjun Hu, Jun Wang. "Study of Ultrasonic Near-Field Region in Ultrasonic Liquid-Level Monitoring System", Micromachines, 2020 Publicación	<1%
37	Submitted to University of Southampton Trabajo del estudiante	<1%
38	docplayer.com.br Fuente de Internet	<1%
39	manualzz.com Fuente de Internet	<1%

40	onlinelibrary.wiley.com Fuente de Internet	<1%
41	etheses.whiterose.ac.uk Fuente de Internet	<1%
42	wikimili.com Fuente de Internet	<1%
43	portlandpress.com Fuente de Internet	<1%
44	eprints.utem.edu.my Fuente de Internet	<1%
45	Submitted to Universiti Teknologi Malaysia Trabajo del estudiante	<1%
46	Submitted to University of Bath Trabajo del estudiante	<1%
47	Aldo Roda, Luca Cevenini, Elisa Michelini, Bruce R. Branchini. "A portable bioluminescence engineered cell-based biosensor for on-site applications", Biosensors and Bioelectronics, 2011 Publicación	<1%
48	Hui Chen, Olja Simoska, Koun Lim, Matteo Grattieri et al. "Fundamentals, Applications, and Future Directions of Bioelectrocatalysis", Chemical Reviews, 2020 Publicación	<1%

49	www.omicsonline.com Fuente de Internet	<1%
50	Inomata, Naoki, Libao Pan, Masaya Toda, and Takahito Ono. "Temperature-depended mechanical properties of microfabricated vanadium oxide mechanical resonators for thermal sensing", Japanese Journal of Applied Physics, 2016. Publicación	<1%
51	"Array Transducers and Beamformers", Imaging in Medical Diagnosis and Therapy, 2015. Publicación	<1%
52	en.wikipedia.org Fuente de Internet	<1%
53	Submitted to Universiti Sains Islam Malaysia Trabajo del estudiante	<1%
54	Kuznetsova, L.A.. "Applications of ultrasound streaming and radiation force in biosensors", Biosensors and Bioelectronics, 20070315 Publicación	<1%
55	Matthew A. Cooper. "A survey of the 2001 to 2005 quartz crystal microbalance biosensor literature: applications of acoustic physics to the analysis of biomolecular interactions", Journal of Molecular Recognition, 05/2007 Publicación	<1%

56	Ngoepe, Mpho, Yahya Choonara, Charu Tyagi, Lomas Tomar, Lisa du Toit, Pradeep Kumar, Valence Ndesendo, and Viness Pillay. "Integration of Biosensors and Drug Delivery Technologies for Early Detection and Chronic Management of Illness", Sensors, 2013. Publicación	<1%
57	Hannes E. Leetaru, Scott M. Frailey, James Damico, Edward Mehnert, Jens Birkholzer, Quanlin Zhou, Preston D. Jordan. "Understanding CO2 Plume Behavior and Basin-Scale Pressure Changes during Sequestration Projects through the use of Reservoir Fluid Modeling", Energy Procedia, 2009 Publicación	<1%
58	Antonia Lopreside, Maria Maddalena Calabretta, Laura Montali, Martina Zangheri et al. "Bioluminescence goes portable: recent advances in whole-cell and cell-free bioluminescent biosensors", Luminescence, 2020 Publicación	<1%
59	Submitted to University of Hull Trabajo del estudiante	<1%
60	Submitted to University of Nottingham Trabajo del estudiante	<1%

61	Nordin, Anis N.. "Label-Free Biochips", Advanced Biomaterials and Biodevices, 2014. Publicación	<1%
62	Kerstin Länge. "Surface acoustic wave biosensors: a review", Analytical and Bioanalytical Chemistry, 07/2008 Publicación	<1%
63	technocraveph.blogspot.com Fuente de Internet	<1%
64	scholarsmine.mst.edu Fuente de Internet	<1%
65	Kirk Shung, . "Ultrasonic Transducers and Arrays", Diagnostic Ultrasound Imaging and Blood Flow Measurements, 2005. Publicación	<1%
66	Daria Wotzka, Tomasz Lusa. "Theoretical study on the phenomena connected with cracking occurring in steel pipe based on multiphysical FE model", Journal of Mechanical Science and Technology, 2015 Publicación	<1%
67	ieeexplore.ieee.org Fuente de Internet	<1%
68	www.jourlib.org Fuente de Internet	<1%

69	research.library.mun.ca Fuente de Internet	<1%
70	publications.lib.chalmers.se Fuente de Internet	<1%
71	Dan I. Piraner, Arash Farhadi, Hunter C. Davis, Di Wu, David Maresca, Jerzy O. Szablowski, Mikhail G. Shapiro. "Going Deeper: Biomolecular Tools for Acoustic and Magnetic Imaging and Control of Cellular Function", Biochemistry, 2017 Publicación	<1%
72	Yann Chevolot. "Carbohydrates as Recognition Receptors in Biosensing Applications", Recognition Receptors in Biosensors, 2010 Publicación	<1%
73	www.centronacionaldeconsultoria.com Fuente de Internet	<1%
74	upcommons.upc.edu Fuente de Internet	<1%
75	www.dtic.mil Fuente de Internet	<1%
76	Voiculescu, I.. "Acoustic wave based MEMS devices for biosensing applications", Biosensors and Bioelectronics, 20120315 Publicación	<1%

77	ARUN K. BHUNIA. "LIGHT SCATTERING, FIBER OPTIC- AND CELL-BASED SENSORS FOR SENSITIVE DETECTION OF FOODBORNE PATHOGENS", Journal of Rapid Methods and Automation in Microbiology, 6/2007 Publicación	<1%
78	bbrc.in Fuente de Internet	<1%
79	hdl.handle.net Fuente de Internet	<1%
80	scholar.uwindsor.ca Fuente de Internet	<1%
81	IFMBE Proceedings, 2010. Publicación	<1%
82	Fan, X.. "Sensitive optical biosensors for unlabeled targets: A review", Analytica Chimica Acta, 20080714 Publicación	<1%
83	www.ncbi.nlm.nih.gov Fuente de Internet	<1%

Excluir citas	Apagado	Excluir coincidencias	Apagado
Excluir bibliografía	Activo		